Online Resource 1

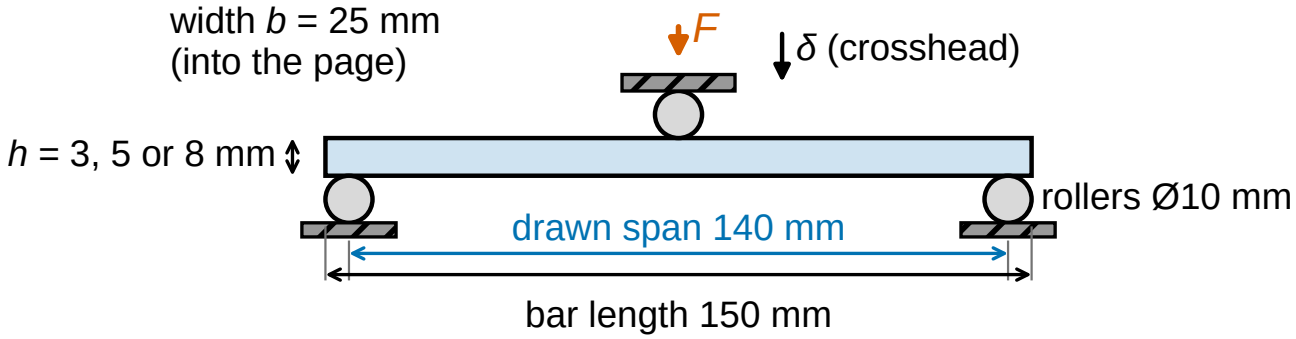
Load recovery at fixed deflection after creep relaxation in bending as a test of anelastic back-stress laws

Yo-Lun Yang

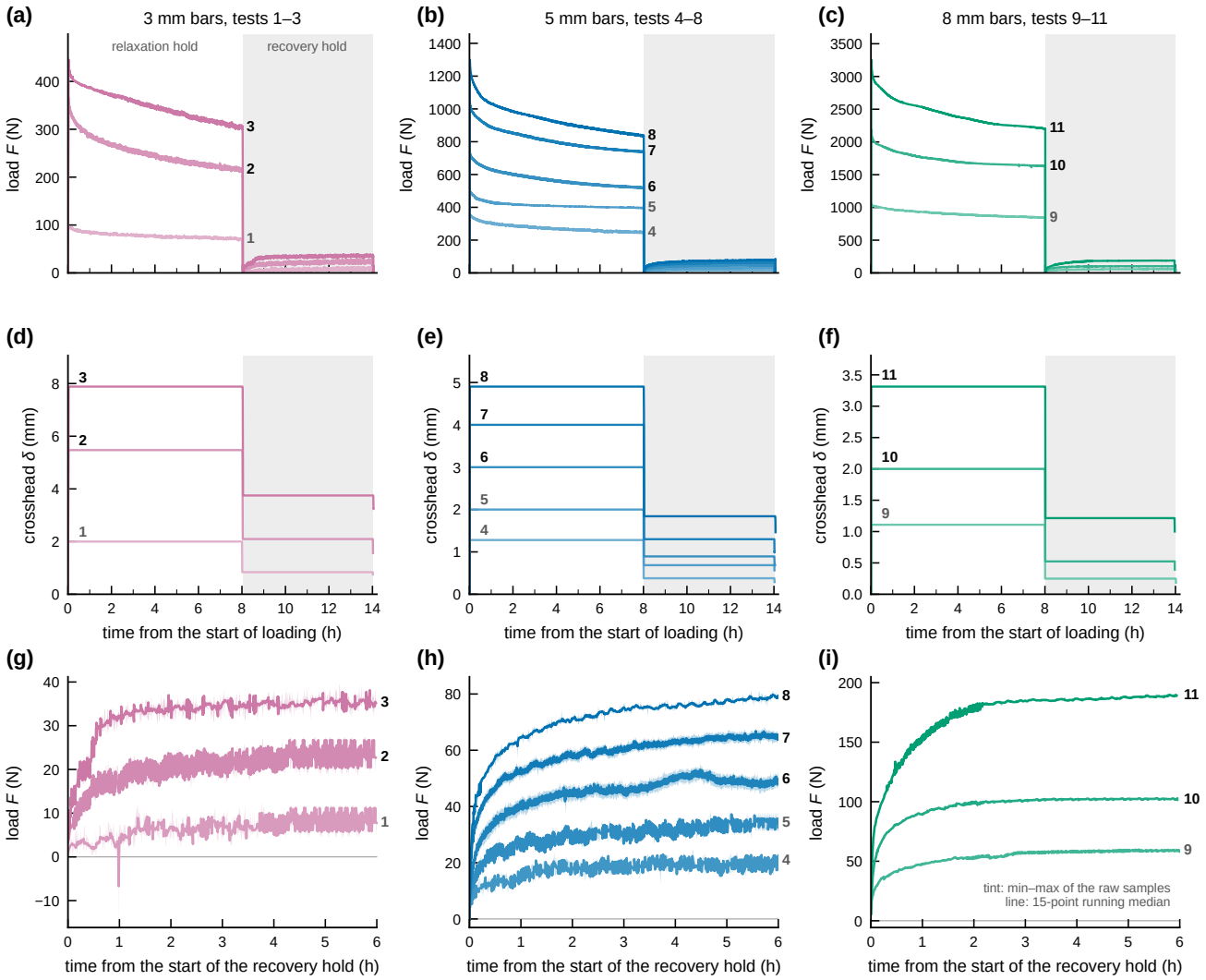
Graduate Institute of Manufacturing Technology, National Taipei University of Technology, 1 Sec. 3 Zhongxiao E. Rd., Taipei 106344, Taiwan

y.yang@ntut.edu.tw

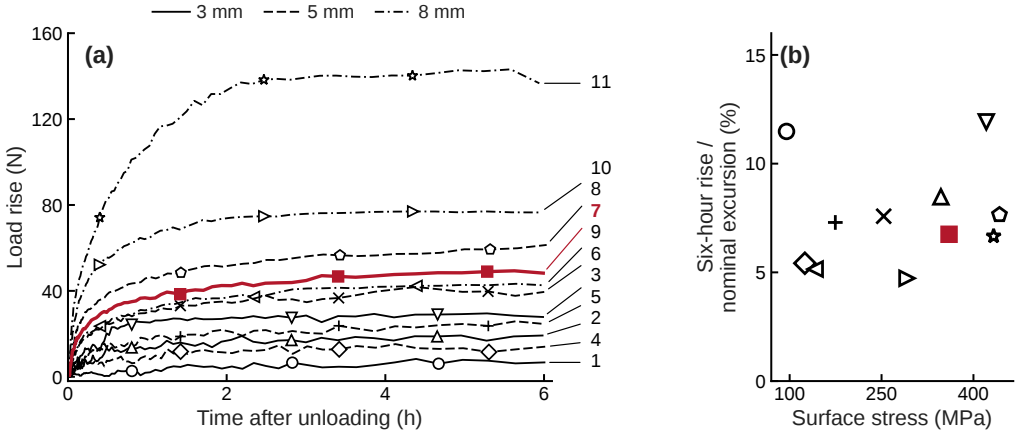
The figures and tables below give the records and calculations underlying the main article. Figure, table and section numbers with an S prefix refer to this file. Other references to sections, tables and equations refer to the main article. Sections S7 to S15 carry the full text and the floats that the main article summarises or cites. References cited in this file are listed at its end and numbered separately from those of the main article.



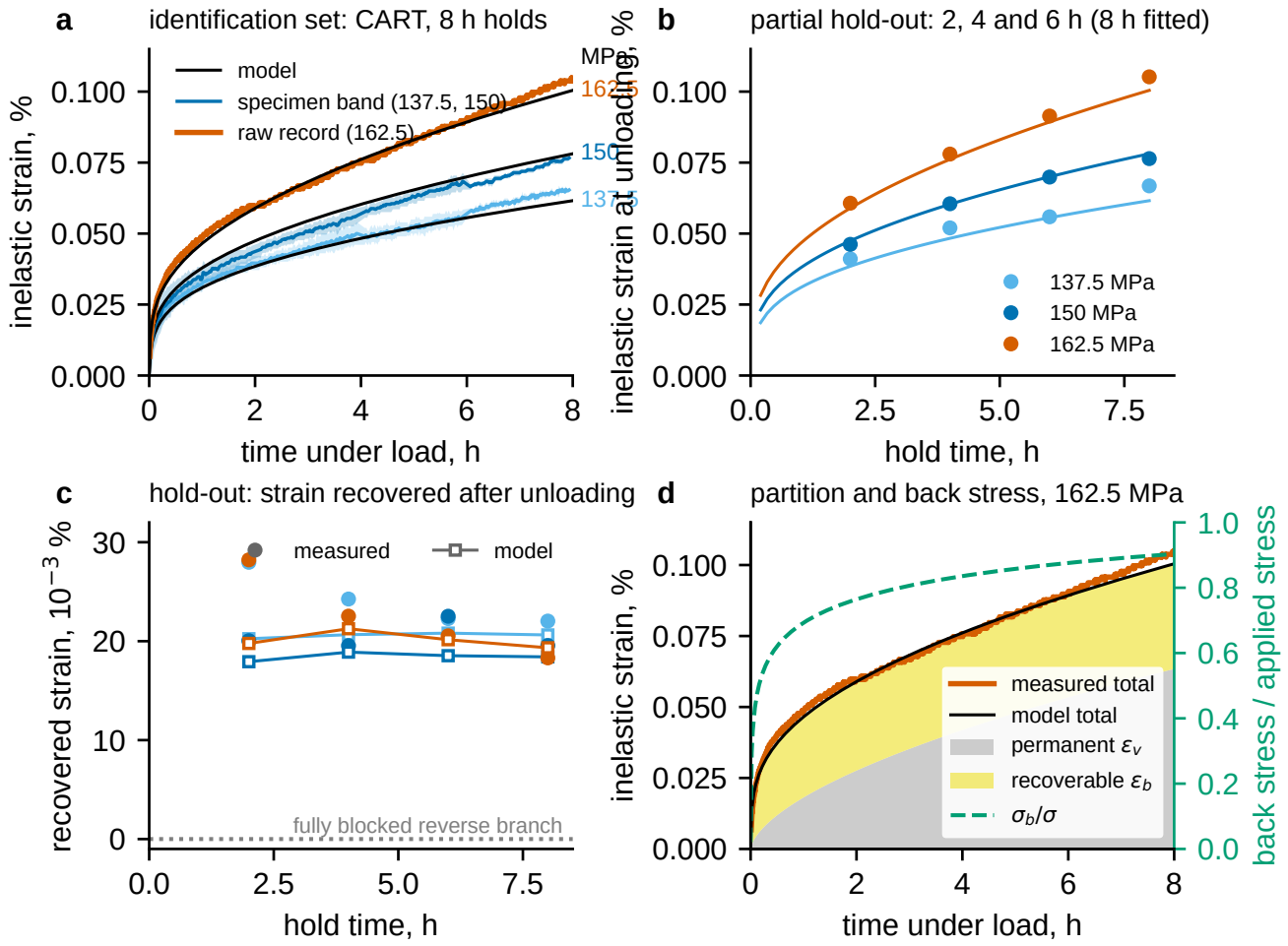
Supplementary Figure S1: Three-point bending rig. The bar of thickness h and width b rests on two rollers at the nominal span and is loaded at mid-span through the crosshead displacement δ. The thickness is drawn for the 8 mm bars.



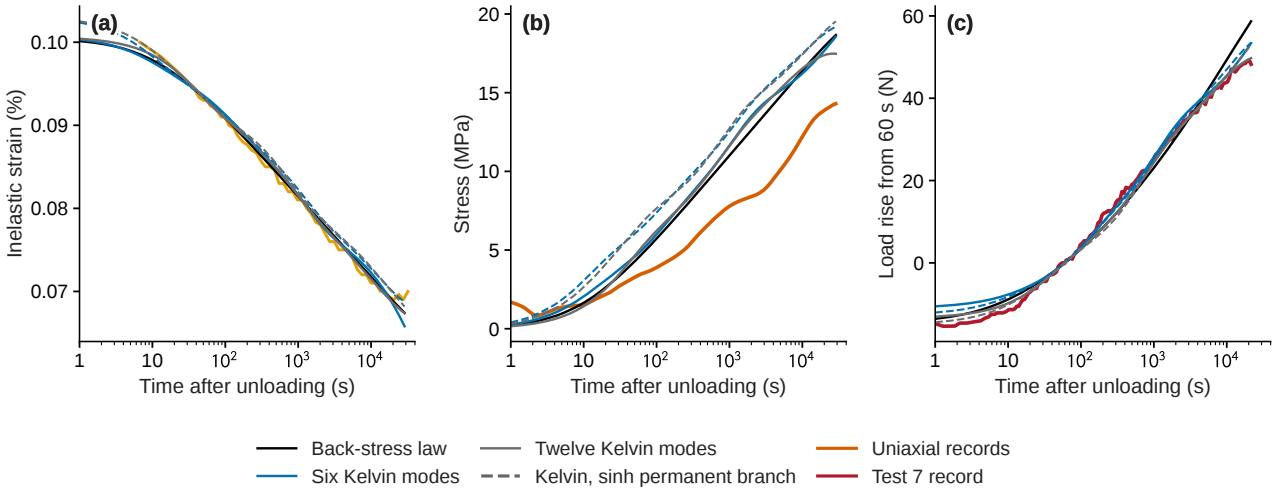
Supplementary Figure S2: Raw records of the eleven SRBT tests, grouped by bar thickness and numbered as in Table 2. (a–c) Load over the whole test, with the 6 hour recovery hold shaded. (d–f) Crosshead displacement, held at δ_0 for 8 hours and at δ_1 for the recovery hold and returned at the end. (g–i) Load during the recovery hold, from the end of the unloading ramp to 2 s before the final movement. The tint spans the minimum and maximum of the raw samples in each time bin and the line is the 15-point running median. Darker shades are higher surface stresses within each thickness. The load of test 1 falls below −2 N once, at 0.99 hours after the start of the hold, for 0.8 s. This record is shown unfiltered here and with that excursion omitted in Fig. 2.



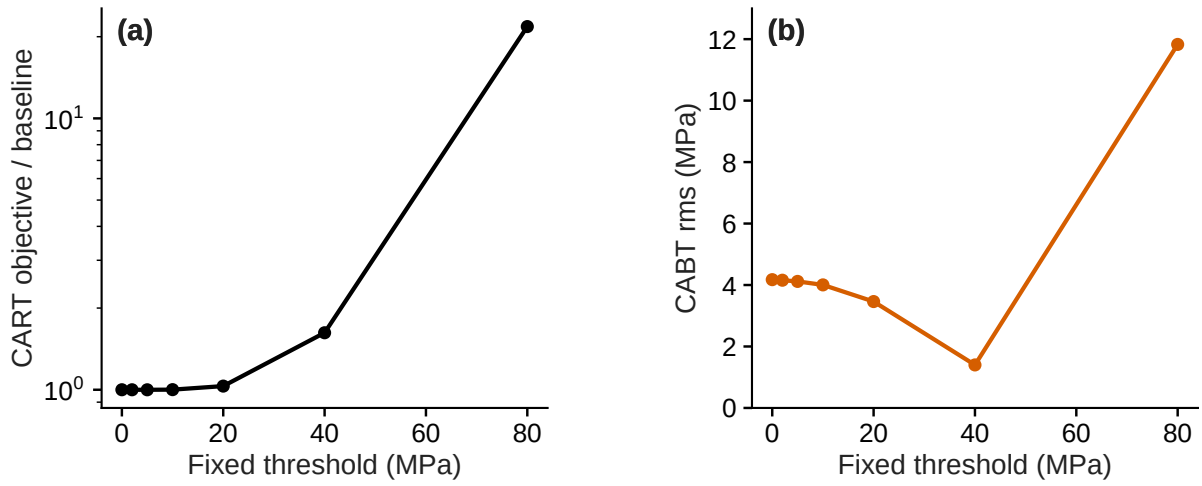
Supplementary Figure S3: Measured load recovery of the eleven bending tests. (a) Rise from the load 60 s after unloading and (b) six-hour rise as a fraction of the nominal unloading excursion $k_0(\delta_0 - \delta_1)$, with $k_0 = F_{\text{app}}/\delta_0$. Line pattern gives the bar thickness and markers follow Fig. 2, with test 7 in red.



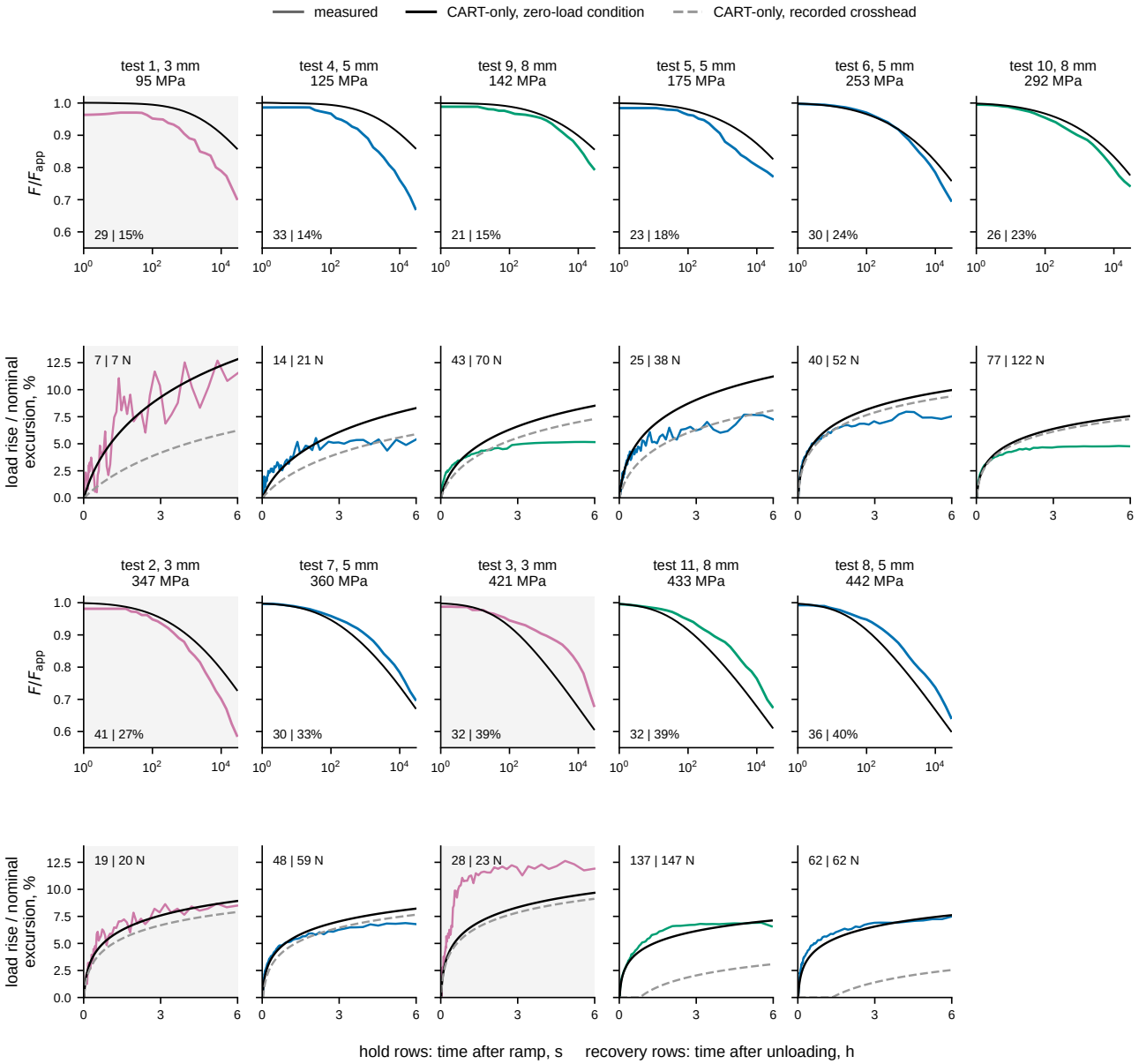
Supplementary Figure S4: Uniaxial identification and hold-outs. (a) The three 8 hour CART holds used for identification, with the specimen band at 137.5 and 150 MPa and the raw record at 162.5 MPa. (b) Inelastic strain at unloading for the twelve CART tests, with the 2, 4 and 6 hour recovery records withheld and their pooled contribution to the identification holds disclosed. (c) Strain recovered after unloading, traced from the first resolved point, measured and predicted, with zero recovery shown as a reference for a fully blocked reverse branch. (d) Partition of the inelastic strain during the 162.5 MPa hold and the ratio of back stress to applied stress.



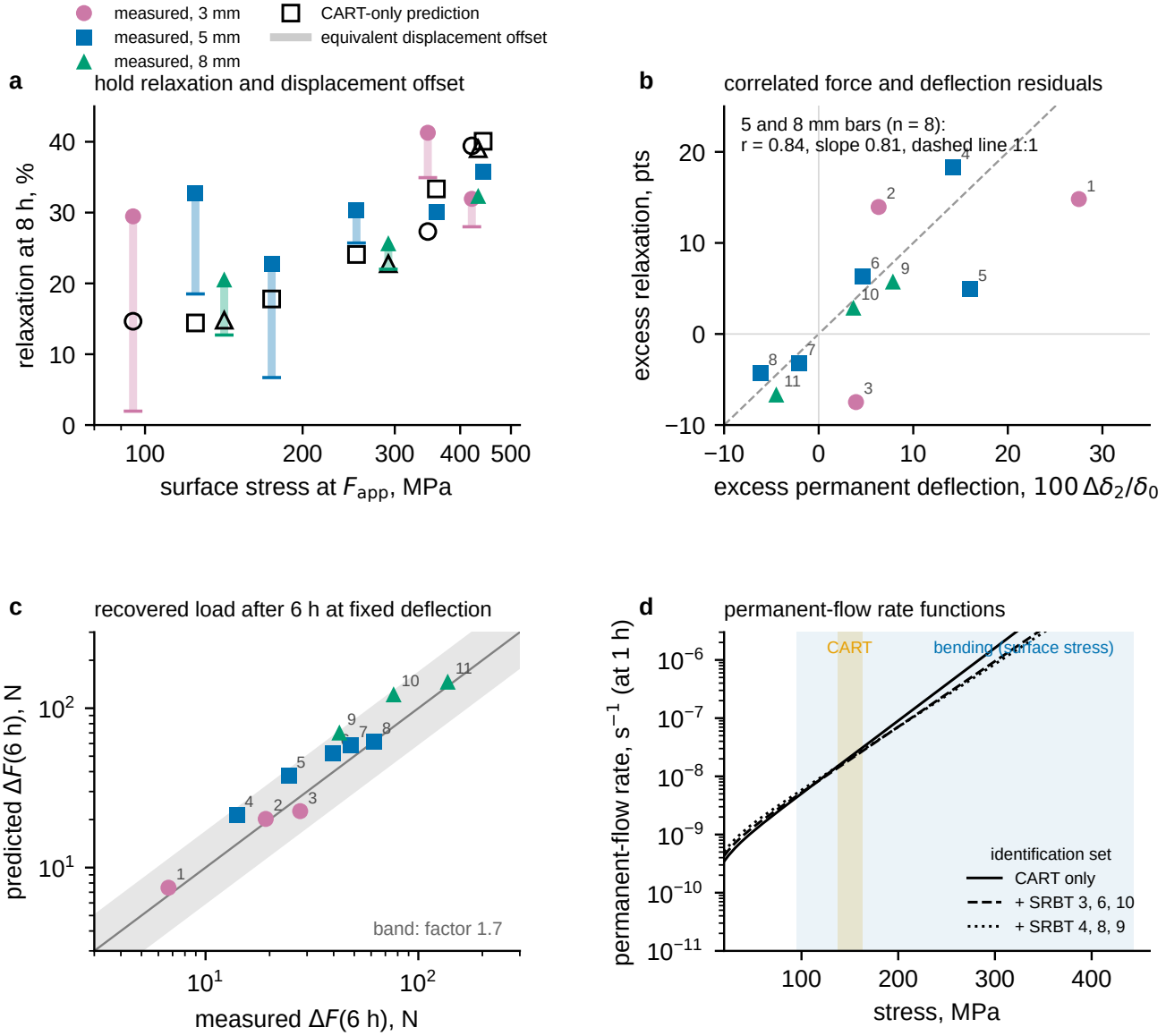
Supplementary Figure S5: Recoverable branches compared under common conditions. Solid lines are the three laws of Table 4 with their own permanent branch, dashed lines the Kelvin spectra with the permanent branch held at the back-stress values. (a) CART identification at 162.5 MPa. (b) CABT assessment. (c) SRBT test 7, each law conditioned to zero load at the end of the unloading ramp, with the load rise measured from 60 s. The coloured CABT curve is a smoothed display trend, and the test 7 record is solid red. Every fit uses CART only.



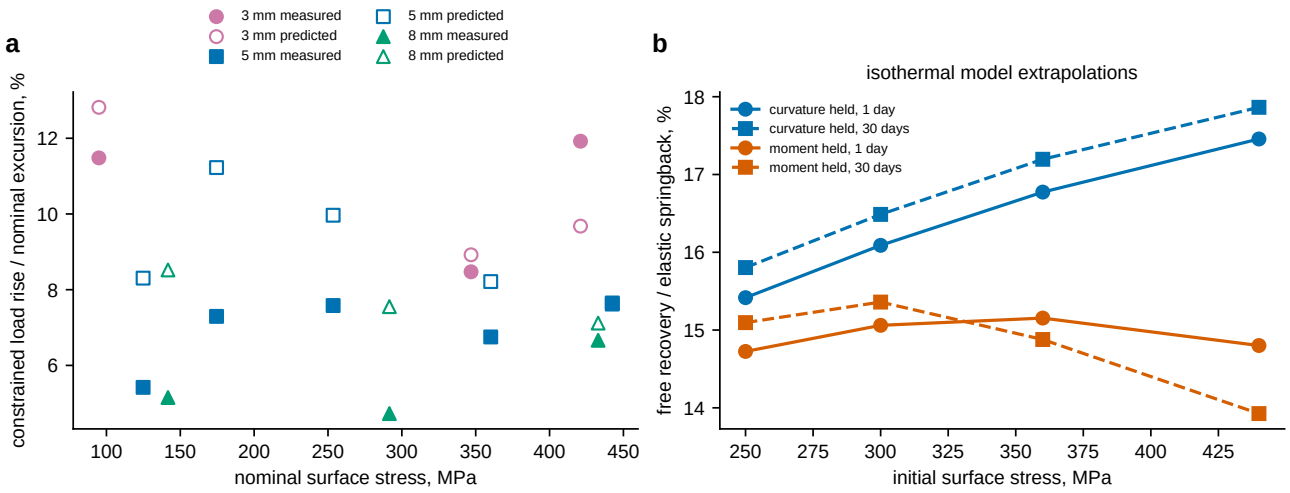
Supplementary Figure S6: Threshold profiles with all six free parameters re-identified on CART at each fixed threshold. (a) CART objective relative to the zero-threshold value. (b) CABT error without further fitting.



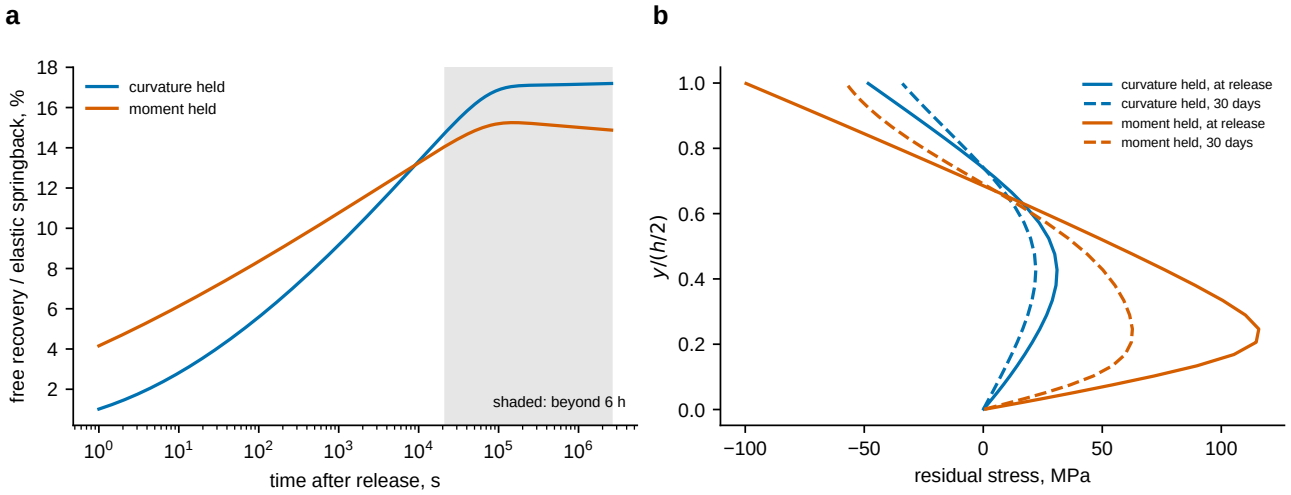
Supplementary Figure S7: Eleven bending tests ordered by nominal surface stress. In each pair of rows the upper panel shows the hold load over the applied load and the lower panel the recovery load rise. The latter is measured from 60 s after unloading, divided by the nominal unloading excursion $k_0(\delta_0 - \delta_1)$, where $k_0 = F_{\text{app}}/\delta_0$. Coloured curves are measured, solid black curves use the CART-only law with the zero-load unloading condition, and dashed curves use the recorded crosshead. Numbers are measured and predicted values. Shading marks the 3 mm bars.



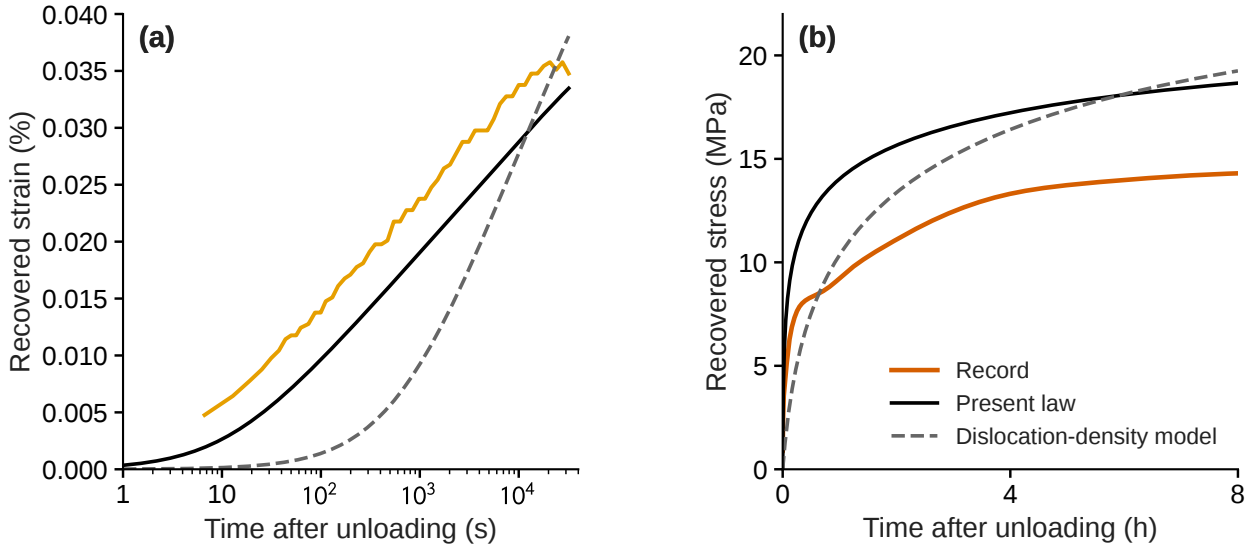
Supplementary Figure S8: Residual diagnostics. (a) Measured hold relaxation, the CART-only prediction and the subtraction of the equivalent displacement offset $100\Delta\delta_2/\delta_0$. (b) Excess relaxation against excess permanent deflection, both relative to the same law. The unit-slope line is what a pure displacement offset would give. (c) Predicted and measured six-hour load rise with the zero-load unloading condition, as in Table S1. (d) Permanent-flow rate functions from the three identifications in Table 3.



Supplementary Figure S9: Different recovery constraints. (a) Six-hour load rise in the constrained three-point tests, normalised by the nominal unloading excursion. Measured and conditionally predicted values are distinguished by marker fill. (b) Calculated free springback at zero moment following constant-curvature or constant-moment forming. One- and thirty-day values are time extrapolations. Reaction recovery and free curvature change are separate observables.



Supplementary Figure S10: Free-release scenarios for a 5 mm section initially loaded to 360 MPa and held for eight hours at constant curvature or constant moment. (a) Calculated delayed springback relative to immediate elastic springback. Shading marks times beyond six hours. (b) Calculated residual stresses at release and thirty days later. Both histories retain the forming temperature and fixed material parameters.



Supplementary Figure S11: The dislocation-density model of Section S8, equations (5.22)–(5.29) with the published constants and no refitting, against the present law on the same records. (a) Strain recovered after unloading from the 162.5 MPa eight-hour creep test, on a logarithmic time axis. Coloured lines denote the records, the black line the present law and the grey dashed line the dislocation-density model. The CABT record is shown as a smoothed display trend. (b) Stress recovered at fixed strain after the same hold. The dislocation-density model reaches the measured recovered strain after eight hours but starts the recovery fifty times more slowly, and its recovered stress exceeds the measured eight-hour reaction.

S1 Results of the individual bending tests

Table S1 summarises the bending outcomes of the CART-only identification, and Table S2 lists the eleven bending tests under the reported evaluation, from which Table S1 and Section 6.3 are drawn.

Supplementary Table S1: Bending outcomes from the CART-only identification. Hold rms error uses thirty points spaced uniformly in $\log t$. The unloading shift u_s is the recorded unloading endpoint minus the model endpoint that gives zero force after reintegration of the unloading ramp. ΔF is the load rise from 60 s to the end of the six-hour recovery hold. $\Delta\delta_2$ is the recorded permanent deflection minus the model inelastic deflection at release, from the residual calculation driven by the recorded crosshead.

test	h (mm)	relax. meas. (%)	relax. pred. (%)	hold rms (p.p.)	u_s (mm)	ΔF meas. (N)	ΔF pred. (N)	$\Delta\delta_2$ (mm)
1	3	29.5	14.7	7.2	0.55	6.7	7.5	0.55
2	3	41.3	27.3	5.3	0.53	19.2	20.2	0.35
3	3	31.9	39.4	7.2	0.42	27.8	22.6	0.31
4	5	32.7	14.4	8.1	0.20	14.0	21.5	0.18
5	5	22.7	17.8	4.1	0.34	24.6	37.8	0.32
6	5	30.4	24.1	2.1	0.15	39.7	52.1	0.14
7	5	30.1	33.3	2.6	-0.08	48.2	58.7	-0.08
8	5	35.8	40.1	4.3	-0.24	62.1	61.9	-0.30
9	8	20.6	14.8	2.4	0.09	42.6	70.4	0.09
10	8	25.7	22.8	2.1	0.06	76.5	122.2	0.07
11	8	32.4	39.0	5.2	-0.14	137.4	146.8	-0.15

Supplementary Table S2: The eleven bending tests calculated with the CART-only parameters under the reported evaluation of Section S13. σ_s is the initial nominal surface stress of Table 2. Peak error is relative to the measured peak load. Hold rms is in percentage points of normalised load at thirty log-spaced times. u_s is the unloading shift of Section 6.3. ΔF is the rise from 60 s to the end of the six-hour recovery. Recovery rms is in % of the nominal unloading excursion. t_{50} is the half-time of the rise from the same baseline. The measured and calculated histories are plotted in Fig. S7.

			peak load (N)		peak	hold		ΔF (N)			recovery	t_{50} (s)		
test	h (mm)	σ_s (MPa)	meas.	calc.	error (%)	rms (p.p.)	u_s (mm)	meas.	calc.	ratio	rms (%)	meas.	calc.	ratio
1	3	95	100.4	122.5	+22.0	7.24	0.555	6.7	7.5	1.116	1.71	4075	5572	1.37
2	3	347	366.9	325.4	-11.3	5.31	0.530	19.2	20.2	1.053	0.56	1423	1996	1.40
3	3	421	445.3	449.6	+1.0	7.22	0.421	27.8	22.6	0.812	2.86	1304	1719	1.32
4	5	125	366.8	353.7	-3.6	8.11	0.197	14.0	21.5	1.532	1.12	1762	5369	3.05
5	5	175	512.9	551.4	+7.5	4.05	0.339	24.6	37.8	1.539	1.53	1467	3179	2.17
6	5	253	744.8	814.8	+9.4	2.09	0.147	39.7	52.1	1.315	0.77	935	2139	2.29
7	5	360	1058.3	1063.7	+0.5	2.61	-0.078	48.2	58.7	1.217	0.50	922	1823	1.98
8	5	442	1300.2	1271.0	-2.2	4.29	-0.242	62.1	61.9	0.996	0.67	873	1706	1.95
9	8	142	1065.6	1144.7	+7.4	2.35	0.090	42.6	70.4	1.654	1.14	1170	4103	3.51
10	8	292	2193.2	2039.3	-7.0	2.06	0.064	76.5	122.2	1.597	0.98	630	2150	3.41
11	8	433	3256.4	3247.3	-0.3	5.17	-0.142	137.4	146.8	1.068	0.45	1271	1679	1.32

S2 Sensitivity of the constants and of the bending ratios

The ranges below vary one choice at a time around the reported identification and evaluation. Profiles refit the remaining free parameters at each grid point from the global minimum and from the neighbouring grid point, four starts each, and are shown in Fig. S12. Leave-one-stress-out refits re-identify all six free parameters on two of the three CART histories. The endpoint conventions change the instant and the load from which the recovery is counted. The apparatus scenarios change the span and the machine compliance of the section model. Every bending calculation here uses LSODA at relative tolerance 10^{-9} and reproduces the reported evaluation of all eleven tests to 1.4×10^{-6} relative.

Re-identified on two of the three CART histories, the law gives mean hold errors of 3.1 to 4.2 percentage points over the 5 and 8 mm bars and 3.9 to 4.9 over all eleven, six-hour ratios of 0.77 to 2.07 and half-time ratios of 1.10 to 3.98. Varying the span from 140 to 146 mm and the machine compliance within its one-standard-deviation limits gives mean hold errors of 3.6 to 4.0 over the 5 and 8 mm bars and moves each six-hour ratio by at most 0.23, with the ranges of tests 1, 2 and 8 crossing unity. A constant load offset cancels in the rise. A drift of 2 N over six hours changes the six-hour ratio by up to 0.47 in test 1 and by 0.02 to 0.26 in the other tests, and lowers the ratio of test 3 to 0.76. Two scenarios that change the conditioning itself are kept outside the ranges and reported in Tables S7 and S8. The secant-compliance envelope replaces the apparatus of the ramp fit by the unloading secants of single records, which include inelastic flow during the ramp, and a one-second shift of the stage instants with re-conditioning changes the event on which the model is conditioned, so that the model lifts off earlier than it does under the recorded stop. Under these two scenarios the six-hour ratio of test 9 is 0.45 and 0.24.

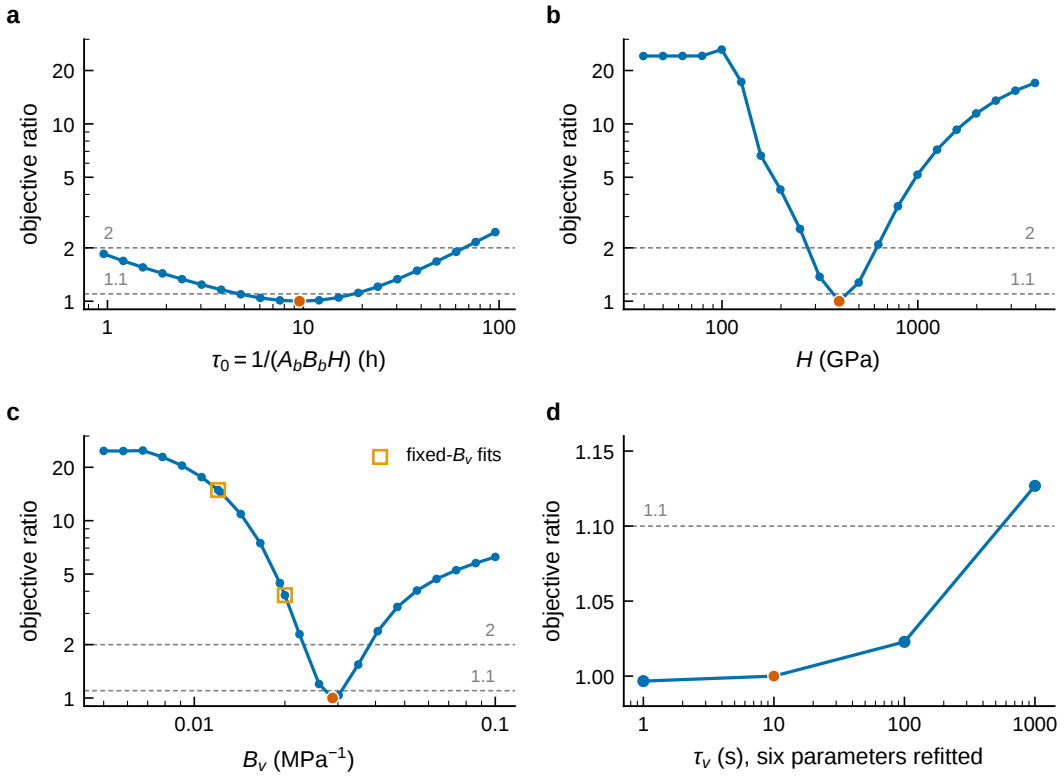
Supplementary Table S3: Ranges of the six identified parameters and of the zero-stress recovery time. Profile ranges are the values over which the CART objective, with every other free parameter re-identified, stays below 1.1 or 2 times its minimum of 1.951. They are read by log-linear interpolation on the profile grid. A < or > sign marks a grid end reached below the threshold. The leave-one-stress-out (LOSO) range spans the three refits on two of the three CART histories. The thresholds are conventions on the objective.

parameter	unit	point value	profile, ratio ≤ 1.1	profile, ratio ≤ 2	LOSO
A_b	s^{-1}	1.24×10^{-9}	6.66×10^{-10} to 2.49×10^{-9}	1.84×10^{-10} to $>1.24 \times 10^{-8}$	9.06×10^{-10} to 2.05×10^{-9}
B_b	MPa^{-1}	0.0591	0.0550 to 0.0613	0.0367 to 0.0774	0.0574 to 0.0595
H	MPa	3.96×10^5	3.73×10^5 to 4.31×10^5	2.79×10^5 to 6.13×10^5	3.92×10^5 to 4.09×10^5
A_v	s^{-1}	6.28×10^{-9}	2.97×10^{-9} to 1.25×10^{-8}	$<6.28 \times 10^{-10}$ to 4.41×10^{-8}	1.54×10^{-9} to 8.31×10^{-9}
B_v	MPa^{-1}	0.0288	0.0274 to 0.0307	0.0233 to 0.0380	0.0279 to 0.0300
p	–	0.408	0.318 to 0.488	<0.102 to 0.650	0.169 to 0.449
$\tau_0 = 1/(A_b B_b H)$	h	9.56	4.70 to 18.1	<0.956 to 66.0	5.97 to 13.1

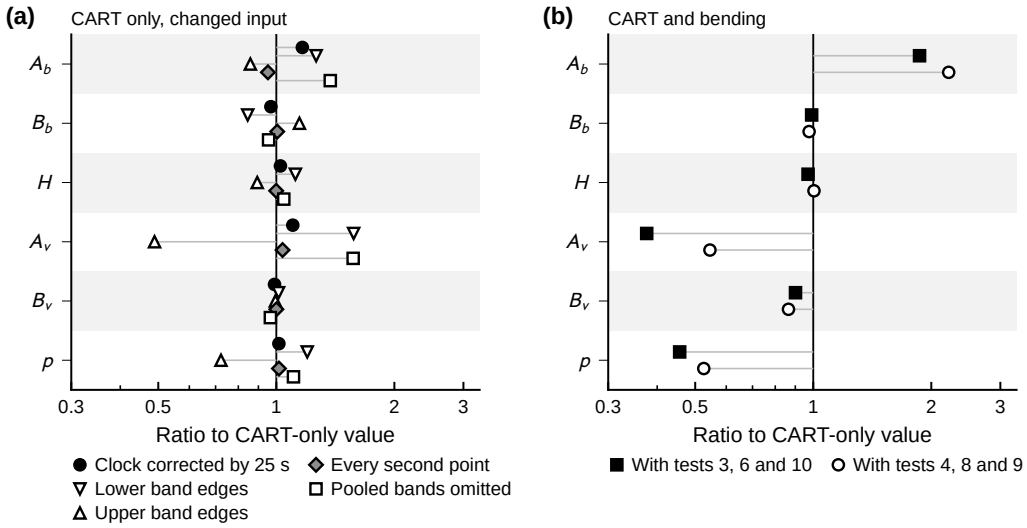
Supplementary Table S4: Refits with the bound on τ_v moved. All six other parameters are re-identified on the 204 CART residuals at each fixed τ_v. Ratio is the objective over its value at $\tau_v = 10$ s.

τ_v (s)	ratio	A_b (s^{-1})	B_b (MPa^{-1})	H (MPa)	A_v (s^{-1})	B_v (MPa^{-1})	p	τ_0 (h)
1	0.9967	1.33×10^{-9}	0.0583	4.02×10^5	1.62×10^{-8}	0.0286	0.406	8.93
10	1.0000	1.24×10^{-9}	0.0591	3.96×10^5	6.28×10^{-9}	0.0288	0.408	9.56
100	1.0228	1.03×10^{-9}	0.0613	3.82×10^5	2.42×10^{-9}	0.0293	0.420	11.48
1000	1.1268	7.61×10^{-10}	0.0648	3.59×10^5	1.02×10^{-9}	0.0302	0.500	15.68

The parameters of the changed-input identifications of Fig. S13a are listed in Table S5.



Supplementary Figure S12: Profiles of the CART objective, as a ratio to its minimum, with every other free parameter re-identified. (a) Zero-stress recovery time $\tau_0 = 1/(A_b B_b H)$. (b) Back-stress stiffness H. (c) Stress sensitivity of the permanent flow B_v, with the two fixed-B_v fits. (d) Fixed τ_v, six parameters refitted. Orange symbols mark the reported identification. Dashed lines mark ratios of 1.1 and 2. The flat ends of panels (b) and (c) are refits with a parameter at a bound.



Supplementary Figure S13: Parameters identified on CART with changed input (a) and jointly with three bending tests (b), as ratios to the CART-only identification, one row per parameter on a common logarithmic scale. The changed inputs correct the acquisition clock of the raw 162.5 MPa record, take either edge of the reconstructed bands, use every second point or omit the pooled hold bands. The joint fits use the recorded crosshead.

Supplementary Table S5: The six-parameter CART identification repeated with its input changed, one change at a time, as plotted in Fig. S13a. Two changes shift the time origin of the 162.5 MPa record by 25 s or take the lower or the upper edge of the reconstructed bands in place of the midpoint. The other two use every second point or omit the two pooled early hold bands. The objective is half the sum of squared residuals over the points listed, so the last two columns are not comparable with the first four. The CABT rms error is over the eight-hour window.

	CART only	25 s shift	lower edge	upper edge	every second point	no pooled bands
A_b (10^{-9} s^{-1})	1.24	1.44	1.56	1.06	1.18	1.70
B_b (MPa^{-1})	0.0591	0.0573	0.0500	0.0677	0.0594	0.0565
H (GPa)	396	406	443	354	396	414
A_v (10^{-9} s^{-1})	6.28	6.92	9.89	3.07	6.51	9.86
B_v (MPa^{-1})	0.0288	0.0285	0.0292	0.0286	0.0288	0.0278
p	0.408	0.414	0.489	0.295	0.414	0.451
points	204	204	204	204	105	154
objective	1.95	2.00	6.45	2.73	0.964	0.689
CABT rms (MPa)	4.17	4.26	2.44	6.16	4.03	4.61

Supplementary Table S6: Leave-one-stress-out refits. Each row re-identifies the six free parameters on two of the three CART histories from eight starts. It then predicts the held-out history and runs the eleven bending tests on the reported protocol. Ratio is the objective of the refit on all three histories over that of the full fit. Held-out rms errors are in % strain, with the full fit in brackets. Bending columns give the mean hold error in percentage points and the six-hour and half-time ratios over the eleven tests. Per-test values are plotted in Fig. 6.

held out (MPa)	ratio	hold rms (%)	recovery rms (%)	τ_0 (h)	p	hold rms 5, 8 mm	hold rms all	six-hour ratio	half-time ratio
none	1	–	–	9.56	0.408	3.84	4.59	0.81 to 1.65	1.32 to 3.51
137.5	1.146	0.00226 (0.00134)	0.00054 (0.00049)	13.10	0.449	4.21	4.93	0.77 to 1.47	1.38 to 3.98
150	1.310	0.00382 (0.00265)	0.00074 (0.00063)	6.59	0.426	3.66	4.40	0.84 to 1.92	1.18 to 3.17
162.5	1.931	0.00407 (0.00185)	0.00104 (0.00076)	5.97	0.169	3.11	3.93	0.88 to 2.07	1.10 to 2.99

Supplementary Table S7: Six-hour and half-time ratios, calculation over record, under the baseline and endpoint conventions. (a) Rise from 60 s after the crosshead stops, as reported. (b) Rise from zero load, the record clock starting at lift-off. Lift-off is the zero of the line fitted to the unloading ramp between 90 and 10 % of the end-of-hold load. (c) As (b) with the record clock starting at the first sample at or below zero load. (d) Convention (a) with the clock origin moved by −1 and +1 s. The last column is the six-hour ratio when the stage instants are moved by −1 s and the model is re-conditioned. The model then lifts off earlier than under the recorded stop, and the case is kept outside the ranges of Fig. 6 as a conditioning choice.

	lift-off	load at	six-hour ratio					half-time ratio			six-hour ratio
test	before stop (s)	lift-off (N)	(a)	(b)	(c)	(d) −1 s	(d) +1 s	(a)	(b)	(c)	stop −1 s
1	1.29	3.0	1.116	0.900	1.131	1.116	1.117	1.37	2.47	1.26	0.582
2	0.75	4.7	1.053	1.040	1.224	1.052	1.051	1.40	1.83	1.04	1.069
3	6.47	25.3	0.812	0.826	0.947	0.813	0.811	1.32	1.22	1.09	0.822
4	0.35	5.1	1.532	1.109	1.398	1.532	1.533	3.05	11.50	5.93	0.360
5	1.74	33.6	1.539	1.174	1.331	1.540	1.537	2.17	6.07	3.10	0.994
6	1.25	19.7	1.315	1.234	1.230	1.317	1.310	2.29	2.65	2.70	1.135
7	1.12	18.7	1.217	1.142	1.163	1.213	1.225	1.98	2.58	2.53	1.200
8	1.14	19.3	0.996	0.980	1.115	0.998	0.995	1.95	2.08	1.32	1.017
9	0.48	25.2	1.654	1.238	1.328	1.655	1.653	3.51	9.63	7.53	0.239
10	0.87	42.7	1.597	1.427	1.540	1.600	1.595	3.41	4.51	3.39	1.139
11	0.79	42.5	1.068	1.050	1.109	1.070	1.071	1.32	1.36	1.08	0.966

Supplementary Table S8: Apparatus scenarios, one at a time around the span and machine stiffness of the ramp fits of Section 2.4. The one-standard-deviation limits are those of the ramp fit. The secant compliances are the smallest and largest positive unloading secants of the individual records, an envelope far wider than the ramp fit. Hold rms in percentage points.

scenario	L (mm)	k_m (N/mm)	hold rms 5, 8 mm	hold rms all	six-hour ratio	half-time ratio
reported	141.8	9467	3.84	4.59	0.81 to 1.65	1.32 to 3.51
span 140 mm	140	9467	3.96	4.69	0.83 to 1.71	1.31 to 3.42
span 146 mm	146	9467	3.58	4.37	0.78 to 1.52	1.34 to 3.72
C_m lower 1 sd limit	141.8	22222	3.95	4.67	0.81 to 1.88	1.30 to 3.28
C_m upper 1 sd limit	141.8	5988	3.73	4.51	0.81 to 1.49	1.32 to 3.76
smallest secant compliance	141.8	11775	3.88	4.62	0.81 to 1.73	1.31 to 3.42
largest secant compliance	141.8	1163	5.76	5.98	0.45 to 1.07	1.33 to 6.15

Supplementary Table S9: Apparatus ranges of the six-hour ratio per test. Span and 1 sd covers the span of 140 to 146 mm and the one-standard-deviation limits of the machine compliance, all scenarios adds the secant envelope. Drift is a linear load drift of ±2 N over the six-hour hold, the order of the record noise of Table 2. A constant load offset cancels in the rise. The last two columns are the largest changes of the predicted peak load and six-hour rise over all scenarios relative to the reported prediction.

test	reported	span and 1 sd	all scenarios	drift ±2 N	peak load (%)	six-hour rise (%)
1	1.116	0.999 to 1.171	0.999 to 1.171	0.860 to 1.590	8.3	10.5
2	1.053	0.996 to 1.078	0.996 to 1.078	0.954 to 1.175	8.0	5.4
3	0.812	0.779 to 0.826	0.777 to 0.826	0.758 to 0.874	7.5	4.3
4	1.532	1.379 to 1.604	1.006 to 1.604	1.341 to 1.787	17.2	34.4
5	1.539	1.410 to 1.597	1.069 to 1.597	1.423 to 1.675	17.1	30.6
6	1.315	1.238 to 1.348	1.004 to 1.348	1.252 to 1.384	16.4	23.6
7	1.217	1.163 to 1.240	0.980 to 1.240	1.168 to 1.269	15.8	19.5
8	0.996	0.958 to 1.013	0.822 to 1.013	0.965 to 1.030	14.9	17.5
9	1.654	1.456 to 1.883	0.450 to 1.883	1.580 to 1.736	43.8	72.8
10	1.597	1.467 to 1.738	0.583 to 1.738	1.557 to 1.640	43.1	63.5
11	1.068	1.005 to 1.137	0.533 to 1.137	1.053 to 1.084	41.2	50.1

Supplementary Table S10: The apparatus figures of Section S13 and their denominators, from the one-at-a-time checks with the CART-only constants among tests 4, 8 and 11.

quantity	value (%)	scenario	relative to
largest change of the six-hour rise	6.4	test 11, L 141.8 mm, C_m 4.50×10^{-5} mm/N	reported prediction
largest change of the peak load	5.4	test 11, L 141.8 mm, C_m 4.50×10^{-5} mm/N	reported prediction
largest peak error	6.8	test 4, L 143.5 mm, C_m 1.06×10^{-4} mm/N	measured peak

Supplementary Table S11: Plotted coordinates of Fig. 6 and the endpoints of its range bars. The load rise is counted from 60 s after the crosshead stops to one hour and to the end of the six-hour hold, for the record (meas.) and for the calculation with the zero-load conditioning (calc.). The half-time is the first time at which the rise reaches half its six-hour value. Each range is the smallest and largest ratio of calculation to record over the choices varied one at a time. The superscript names the choice that sets the endpoint. L is one CART history left out of the identification (Table S6) and E the baseline and endpoint conventions (a) to (d) of Table S7. A is the span of 140 to 146 mm and the one-standard-deviation limits of the machine compliance (Table S9). D is a linear drift of ±2 N over the six-hour hold, applied to the load rise only. The bars in Fig. 6 are drawn at the measured value times these ratios. The secant-compliance envelope of the individual records and the scenario that moves the stage instants by one second are conditioning choices kept outside the ranges (Tables S7 and S8, Section S13).

		rise at 1 h (N)				rise at 6 h (N)				half-time (s)			
test	h (mm)	meas.	calc.	ratio	range	meas.	calc.	ratio	range	meas.	calc.	ratio	range
1	3	1.5	2.8	1.84	0.90^{E} to 2.89^{L}	6.7	7.5	1.12	0.86^{D} to 1.59^{D}	4075	5572	1.37	1.10^{L} to 2.47^{E}
2	3	12.9	12.4	0.97	0.88^{L} to 1.22^{E}	19.2	20.2	1.05	0.95^{D} to 1.22^{E}	1423	1996	1.40	1.04^{E} to 1.83^{E}
3	3	25.3	14.5	0.57	0.54^{L} to 0.74^{E}	27.8	22.6	0.81	0.76^{D} to 0.95^{E}	1304	1719	1.32	1.09^{E} to 1.38^{L}
4	5	9.7	8.4	0.87	0.57^{E} to 1.33^{L}	14.0	21.5	1.53	1.11^{E} to 2.03^{L}	1762	5369	3.05	2.46^{L} to 11.50^{E}
5	5	17.1	20.0	1.17	0.89^{E} to 1.50^{L}	24.6	37.8	1.54	1.17^{E} to 1.84^{L}	1467	3179	2.17	1.81^{L} to 6.07^{E}
6	5	30.4	31.5	1.04	0.93^{L} to 1.21^{L}	39.7	52.1	1.31	1.21^{L} to 1.48^{L}	935	2139	2.29	2.01^{L} to 2.70^{E}
7	5	37.1	37.0	1.00	0.92^{L} to 1.14^{L}	48.2	58.7	1.22	1.14^{E} to 1.34^{L}	922	1823	1.98	1.78^{L} to 2.58^{E}
8	5	46.5	39.7	0.85	0.79^{E} to 1.03^{E}	62.1	61.9	1.00	0.95^{L} to 1.12^{E}	873	1706	1.95	1.32^{E} to 2.08^{E}
9	8	31.5	33.0	1.05	0.74^{E} to 1.45^{L}	42.6	70.4	1.65	1.24^{E} to 2.07^{L}	1170	4103	3.51	2.86^{L} to 9.63^{E}
10	8	64.3	73.8	1.15	1.04^{L} to 1.35^{L}	76.5	122.2	1.60	1.43^{E} to 1.80^{L}	630	2150	3.41	2.99^{L} to 4.51^{E}
11	8	107.6	94.6	0.88	0.82^{L} to 0.99^{L}	137.4	146.8	1.07	1.00^{A} to 1.16^{L}	1271	1679	1.32	1.08^{E} to 1.39^{L}

S3 Sensitivity of the residuals

Supplementary Table S12: Conditional local parameter scales, in % of each parameter, from the information matrix at the CART-only parameters. Each block is weighted by the rms of its residual. The CABT weight uses the stress record at thirty logarithmically spaced times from 300 s to 8 h. One local scale corresponds to an objective ratio of 1.0049 on the CART block.

design	A_b	B_b	H	A_v	B_v	p	condition number
CART	14.6	2.32	2.86	15.6	1.69	4.55	$1.84 \times 10^{+5}$
CART + CABT	14.1	2.3	2.84	15.6	1.66	4.43	$1.83 \times 10^{+5}$
CART + eight bars	5.42	1.56	1.89	13.8	1.18	4.11	$1.12 \times 10^{+5}$
all four blocks	5.41	1.54	1.87	13.6	1.18	4.04	$1.09 \times 10^{+5}$
CART + eleven bars	5.17	1.54	1.82	13.7	1.16	4.12	$1.08 \times 10^{+5}$
all, eleven bars	5.17	1.52	1.81	13.5	1.16	4.05	$1.05 \times 10^{+5}$

The weights of the four residual blocks and the correlations of the CART block are listed in Table S13.

Supplementary Table S13: Residual blocks of the information matrix of Section S3, with the rms residual of each block at the CART-only parameters, which is its weight. The correlations of the CART block are those quoted in Section 7.2. The last row gives the share of the diagonal information on A_b that the two bending blocks supply when all four blocks are combined.

block	residual	points	weight
CART	strain on the three identification histories	204	0.0014 %
CABT	stress at fixed strain, 30 times from 300 s to 8 h	30	3.9 MPa
bending hold	normalised load, eight 5 and 8 mm bars, 30 times each	240	4.3 percentage points
bending recovery	load rise over the nominal unloading excursion, 30 times each	240	1.0 %
correlations of the CART block: $r(A_b, B_b) = -0.87$, $r(A_b, H) = 0.81$, $r(A_v, p) = 0.83$			
share of the diagonal information on A_b from the bending blocks, all four blocks: 36 %			

S4 Equations of the dislocation-density model

The dislocation-density model of Section S8 is run from Eqs. (5.22) to (5.29) of Chapter 5 of Yang (2017), with the constants of its Table 5.4 and the initial values of its Table 5.3, uniaxially and without refitting. In the notation of that study, with ε_c the creep strain, $\bar{\rho}_m$ and $\bar{\rho}_i$ the normalised mobile and immobile dislocation densities, $\bar{r}$ the normalised precipitate radius, σ_A the ageing strength and σ_{dis} the dislocation strength,

$$\dot{\varepsilon}_c = A_1 \sinh[B_1(\sigma - n_0\sigma_b)(1 - \bar{\rho}_m)], \tag{S1}$$

$$\dot{\bar{\rho}}_m = A_3(1 - |\bar{\rho}_m|)\,\dot{\varepsilon}_c - C_p|\bar{\rho}_m|^{m_5}\operatorname{sgn}\bar{\rho}_m, \tag{S2}$$

$$\sigma_b = D_2\,\bar{\rho}_m^{n_x}, \tag{S3}$$

$$\dot{\bar{r}} = C_r(Q - \bar{r})^{m_3}(1 + r_0\bar{\rho}_m^{m_4}), \tag{S4}$$

$$\dot{\sigma}_A = C_A\,\dot{\bar{r}}^{m_1}(1 - \bar{r}), \tag{S5}$$

$$\sigma_y = \sigma_{ss} + (\sigma_A^2 + \sigma_{dis}^2)^{1/2}, \tag{S6}$$

$$\dot{\bar{\rho}}_i = A_4\bar{\rho}_m\,\dot{\varepsilon}_c - A_5\sigma_y\bar{\rho}_i^{3/2}, \tag{S7}$$

$$\sigma_{dis} = A_2\,\bar{\rho}_i^{n}. \tag{S8}$$

Equations (S3) and (S8) are the integrated forms of the printed rate equations, with zero initial values. The back stress enters the creep rate through $n_0\sigma_b$ and saturates at σ/n_0 during the hold. The constants are listed in Table S14 and the four ambiguities of the printed equations in Table S15. Integration uses LSODA at relative tolerance 10^{-9} with a maximum step of 60 s. Figure S11 compares the model with the records.

Supplementary Table S14: The nineteen constants of the dislocation-density model as printed in Table 5.4 of Yang (2017), with the equation in which each appears. The source prints no units. The constants are used with time in hours, stress in MPa and strain dimensionless. Under that convention alone they reproduce the creep and recovery magnitudes of Fig. 5.5 of that study. The initial values of Table 5.3 are $\varepsilon_c = 0$, $\bar{\rho}_m = 0$, $\bar{r} = 1$, $\sigma_A = 300\,\mathrm{MPa}$, $\sigma_{ss} = 273\,\mathrm{MPa}$ and $\bar{\rho}_i = 0$.

constant	value	Eq.	constant	value	Eq.
A_1	9.87×10^{-6}	5.22	m_3	1.3	5.25
B_1	0.054	5.22	m_4	2.4	5.25
n_0	6.6	5.22	Y_0	40.7	5.25 (r_0)
A_3	316	5.23	C_A	80.2	5.26
C_p	2988	5.23	m_1	0.97	5.26
m_5	6	5.23	A_4	50	5.28
D_2	124.8	5.24	A_5	0.001	5.28
n_x	1.07	5.24	A_2	10	5.29
C_r	0.037	5.25	n	0.1	5.29
Q	5	5.25			

Supplementary Table S15: The four places where the printed equations admit more than one reading, and the reading used. The last column is the CART objective of the dislocation-density model on the 204 residuals of the present identification under the alternative reading, with the printed constants and no refitting. Under the readings used the objective is 147.19. Equations 5.25 to 5.29 do not enter Eqs. 5.22 to 5.24, so creep, recovery and back stress depend on eight constants only.

Eq.	ambiguity	reading used	objective, alternative
5.24	power of $\bar{\rho}_m$ if $\bar{\rho}_m < 0$	$\mathrm{sgn}(\bar{\rho}_m)\lvert\bar{\rho}_m\rvert^{n_x}$	147.19, $\bar{\rho}_m$ stays nonnegative
5.25	r_0 absent from Table 5.4	$r_0 = Y_0 = 40.7$, the only unassigned printed constant	unchanged, no feedback
5.26	$(\mathrm{d}\bar{r}/\mathrm{d}t)^{m_1}$ or $m_1 \bar{r}^{m_1-1}\,\mathrm{d}\bar{r}/\mathrm{d}t$	the first, as printed	147.19
5.28	$\bar{\rho}_m$ times the creep rate or the creep strain	the rate, as printed in a rate equation	147.19

S5 Effect of hold duration

Table S16 sets the strain recovered after CART holds of 2, 4, 6 and 8 hours against the present law and against the dislocation-density model of Section S8, both run without refitting (Fig. 8). Recovery is counted from unloading to the end of each record, and every value uses the window of its own record, which runs from 6.0–13.3 h after unloading. The measured recovery rises from the 2 to the 4 hour hold at 137.5 and 150 MPa and falls at 162.5 MPa, and after 8 hours it lies 11, 23 and 17 % below the 2 hour value. The feature common to the three stresses is that the recovery shows no sustained growth beyond four hours. On the common six-hour window of Table 1 the recovered strain falls from 0.034 to 0.031, from 0.036 to 0.026 and from 0.042 to 0.036 % between the 2 and the 8 hour holds, so the trend does not depend on the unequal record lengths. The law rises at every step, by 17, 29 and 20 % from 2 to 8 hours, because its back stress is still growing at the end of the hold and a longer hold stores more recoverable strain. The dislocation-density model changes by −5.8, +10.0 and +0.4 %, because its back stress has saturated by two hours. After the 2 hour holds the law recovers 0.0229–0.0274 % against 0.0361–0.0431 % measured, a deficit that contains the fast component of Section 4.4, and the dislocation-density model comes closer in magnitude by the slower early path described in Section S8.

Table 1 lists the raw 162.5 MPa record after the 8 hour hold to 8.9 h, whereas its traced record ends at 7.9 h. On the 8.9 h window the law recovers 0.0335 % after that hold and its change from the 2 hour hold is 22.0 % instead of 20.5. At the other tests the two windows agree to within 0.12 h. The dependence bounds the recovered strain and not the back stress, since a change in the stiffness or in the kinetics of the recoverable element during the hold would alter the recovered strain as much as a change in the stored stress, and Section 9.1 sets out the candidates.

Supplementary Table S16: Strain recovered from unloading to the end of each record after the 2, 4, 6 and 8 hour CART holds, in %. The last column is its change from the 2 to the 8 hour hold. The present law and the dislocation-density model of Section S8 are run without refitting, each on the window of its own record.

	σ (MPa)	2 h	4 h	6 h	8 h	change (%)
measured	137.5	0.0369	0.0381	0.0359	0.0329	−10.8
	150	0.0361	0.0444	0.0414	0.0279	−22.6
	162.5	0.0431	0.0394	0.0342	0.0359	−16.8
present law	137.5	0.0229	0.0254	0.0265	0.0268	+17.0
	150	0.0232	0.0260	0.0277	0.0299	+29.2
	162.5	0.0274	0.0311	0.0322	0.0331	+20.5
dislocation-density model	137.5	0.0348	0.0358	0.0346	0.0328	−5.8
	150	0.0318	0.0326	0.0326	0.0350	+10.0
	162.5	0.0370	0.0390	0.0378	0.0372	+0.4

Supplementary Table S17: Strain recovered from unloading to the end of each record after the 2 and 8 hour CART holds, in %, and its change between the two holds. The ageing-stiffness variant $H = H_0(1 + t/3600\,\mathrm{s})^q$ of Section 9.1 is set beside the measured values and the present law of Table S16, on the same record windows. The variant is refitted on the same 204 residuals.

	measured			present law			ageing-stiffness variant		
σ (MPa)	2 h	8 h	change (%)	2 h	8 h	change (%)	2 h	8 h	change (%)
137.5	0.0369	0.0329	-10.8	0.0229	0.0268	+17.0	0.0255	0.0273	+7.2
150	0.0361	0.0279	-22.6	0.0232	0.0299	+29.2	0.0258	0.0309	+20.0
162.5	0.0431	0.0359	-16.8	0.0274	0.0331	+20.5	0.0313	0.0345	+10.1

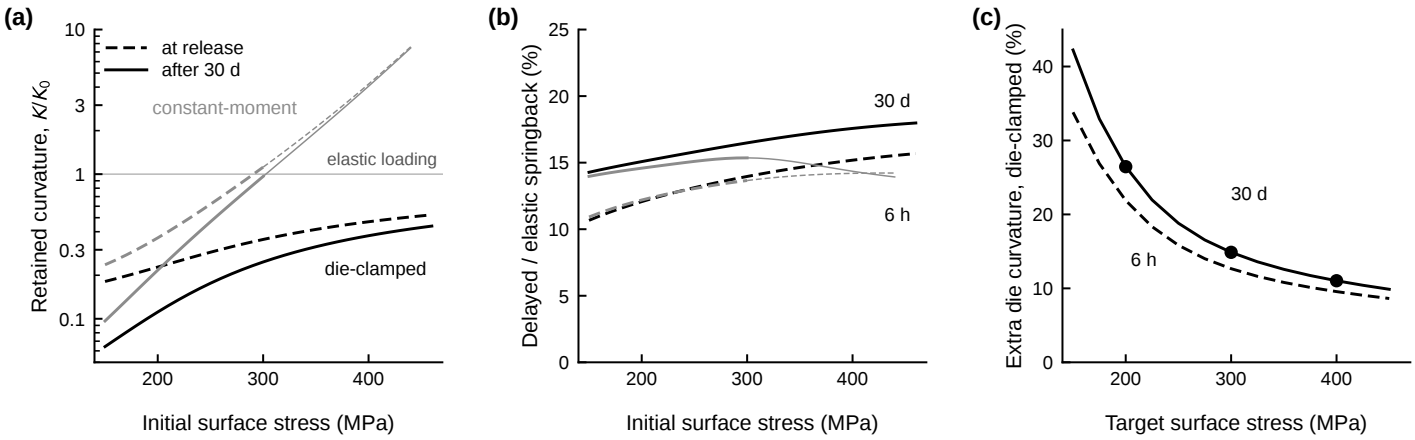
The CABT error of the ageing-stiffness variant is set beside those of the CART-only and joint identifications in Table S18.

Supplementary Table S18: Rms error of the stress at fixed strain over the eight-hour CABT window for the identifications of the main text, evaluated at uniform 3 s intervals as in Section 2.3.

identification	CABT rms (MPa)
CART only (Table 3, row 1)	4.17
CART + SRBT 3, 6, 10 (row 2)	6.91
CART + SRBT 4, 8, 9 (row 3)	6.95
ageing-stiffness variant, $H = H_0(1 + t/3600\,\mathrm{s})^q$, $q = 0.22$	5.20

S6 Free springback and die compensation

The map of Fig. S14 and Table S19 extends the four stresses of Table 6, and Table S20 repeats the forming calculations with the parameter sets of Tables 3 and 5.



Supplementary Figure S14: Conversion between the two holds and the die compensation, from the section model of Table 6 over a continuous range of initial surface stress, with temperature and constitutive parameters fixed. The dimensionless results hold for every section thickness. (a) Curvature at release (dashed) and after thirty days (solid) relative to the elastic curvature at loading, for the die-clamped hold (black) and the constant-moment hold (grey). (b) Delayed springback at six hours (dashed) and at thirty days (solid) as a fraction of the elastic springback at release for both holds. (c) Additional die curvature needed for a die-clamped hold to retain the target release curvature when assessed at six hours (dashed) or at thirty days (solid). Circles mark the three targets of the text. Constant-moment results above 300 MPa, drawn thin, lie beyond the identification set. The returning moment in six hours when the release curvature is held is listed in Table S19.

Supplementary Table S19: Values of the process map of Fig. S14 at 50 MPa intervals, from the pure-bending section model of Table 6 with temperature and constitutive parameters fixed. K_{rel} and K_{30} are the curvatures at release and after thirty days and K_0 the elastic curvature at loading. Springback S is the delayed springback as a percentage of the elastic springback at release. M_6 is the returning moment in six hours when the release curvature is held after the die-clamped hold. It is given in % of the moment released at the end of the hold. The constant-moment sweep ends at 440 MPa. The compensation columns give the additional die curvature, in %, for a die-clamped hold whose target surface stress is the first column. It is assessed at six hours or thirty days. The map is dimensionless and holds for every section thickness.

	die-clamped hold					constant-moment hold			compensation (%)	
σ_{s0} (MPa)	K_{rel}/K_0	K_{30}/K_0	$S_{6\,\mathrm{h}}$ (%)	$S_{30\,\mathrm{d}}$ (%)	M_6 (%)	K_{rel}/K_0	$S_{6\,\mathrm{h}}$ (%)	$S_{30\,\mathrm{d}}$ (%)	6 h	30 d
150	0.181	0.064	10.7	14.3	9.5	0.236	10.9	14.0	33.8	42.2
200	0.228	0.111	12.1	15.1	10.6	0.363	12.2	14.6	21.9	26.5
250	0.289	0.176	13.1	15.8	11.5	0.619	13.1	15.1	15.8	18.8
300	0.354	0.247	14.0	16.5	12.2	1.118	13.7	15.4	12.7	14.9
350	0.415	0.315	14.6	17.1	12.7	2.109	14.0	15.0	10.8	12.6
400	0.469	0.375	15.2	17.6	13.2	4.197	14.2	14.4	9.6	11.0
450	0.515	0.428	15.6	17.9	13.5	–	–	–	8.6	9.9

Supplementary Table S20: Free-release and die-compensation results of Section 8 recomputed with the alternative parameter sets of Tables 3 and 5, with the same section model, hold and temperature. S is the delayed springback of the die-clamped 5 mm section as a percentage of the elastic springback at release. It is given at six hours and at thirty days for initial surface stresses of 250 and 440 MPa. The compensation columns give the additional die curvature, in %, that retains the release curvature of the target surface stress when judged at six hours or thirty days. The sets are the CART-only identification, the three leave-one-stress-out (LOSO) refits and the two joint identifications with bending tests.

	τ_0	S, 250 MPa (%)		S, 440 MPa (%)		compensation, 6 h (%)			compensation, 30 d (%)		
identification set	(h)	6 h	30 d	6 h	30 d	150 MPa	300 MPa	450 MPa	150 MPa	300 MPa	450 MPa
CART only	9.6	13.1	15.8	15.5	17.9	33.8	12.7	8.6	42.2	14.9	9.9
LOSO, without 137.5 MPa	13.1	12.0	15.3	14.8	17.7	30.0	11.6	8.2	40.7	14.3	9.8
LOSO, without 150 MPa	6.6	13.9	15.8	15.5	17.3	36.6	13.1	8.6	42.5	14.7	9.5
LOSO, without 162.5 MPa	6.0	15.1	16.9	16.9	18.5	40.2	14.5	9.4	45.7	16.1	10.3
joint, SRBT 3, 6, 10	5.3	15.7	17.4	17.3	18.8	42.4	15.5	9.8	47.4	16.9	10.7
joint, SRBT 4, 8, 9	4.4	15.6	16.9	16.9	18.0	42.6	15.3	9.6	46.4	16.5	10.3

S7 Experimental details

S7.1 Material and apparatus

The apparatus description and Fig. 3.8 of the earlier study identify an Instron 2620-601 dynamic extensometer for CART and CABT. A later CABT paragraph instead names the 2630-107 used for tensile testing.

S7.2 Data reduction

The raw CART record at 162.5 MPa and 8 hours, sampled every 6.2 s, is the primary uniaxial record. The strain channel is quantised in steps of 0.00033 % and its noise, the standard deviation about a 15-point running median between 6 and 8 hours after unloading, is 0.0002 %. In the strain channel the elastic strain σ/E is reached by the reading at 30 s after the start of loading and the unloading is a single step, from 0.354 % to 0.106 % between two consecutive readings 6.5 s apart. The step fixes the modulus at 65.5 GPa, 0.5 % above the value used here, and the origin of the time after unloading. After unloading the strain falls to 0.069 % at 6 hours, reaches a minimum of 0.068 % at 7.5 hours and ends at 0.070 %, 8.9 hours after unloading.

The other eleven CART records were read from the plotted records of the earlier study (Yang, 2017). Each recovery curve was traced individually, with its first reading 2.7 to 5.6 minutes after unloading. The 8 hour holds at 137.5 and 150 MPa were traced from the plots as well. At each stress the plot overlays the holds of the 2, 4, 6 and 8 hour tests, so four specimens are on load until 1.93 hours, three until 3.93 hours, two until 5.92 hours and one thereafter. The hold curve at each stress was taken as the midpoint of the band of specimens still on load, and the width of the band was kept as the specimen-to-specimen scatter. At 162.5 MPa the midpoint agrees with the raw record to 0.0007 % rms and 0.0017 % at most over the 468 points of the band, which is the scale of the tracing error. Inelastic strain is the measured strain less σ/E.

The CABT record of the earlier study (Yang, 2017) contains 26 245 paired samples through loading, the hold, unloading and recovery, with intervals no longer than 3 s. Recovery time is counted from the local load minimum at 28 844.122 s, which is used to locate the end of unloading. The record continues for 13.5 hours after this point, and comparisons use the first eight hours. The stress reaches 13.6 MPa after four hours and 14.4 MPa after eight hours, with a further rise outside the comparison window. CABT rms errors are evaluated at uniform 3 s intervals over the eight-hour window, interpolating the stored observations between samples.

The eleven bending tests recorded time, crosshead displacement and load through every stage (Fig. S2). The median sampling interval of a record lies between 0.10 and 2.35 s, which gives 10 520 to 505 840 points per record, and the standard deviation of the load about its running median in the last ten minutes of the recovery hold is 0.7–3.6 N. Both ramps ran at 0.06667 mm/s in every test. The relaxation holds lasted 8 hours to within 0.3 s, the recovery holds between 5.94 and 6.03 hours, and the crosshead moved by less than 1×10^{-4} mm during a recovery hold. The final movement ran at a median of 0.0171 mm/s, between 0.0168 and 0.0180 mm/s in ten tests and at 0.0254 mm/s in test 2. During the recovery hold the load rises by 3.5–6.7 % of F_{app}.

The reduction of each bending record follows the stages of the programme. F_{app} and $F_{8\mathrm{h}}$ are the loads at the end of the first ramp and at the end of the relaxation hold, and the relaxation is $1 - F_{8\mathrm{h}}/F_{\mathrm{app}}$. The deflection δ_1 is the crosshead position at which the unloading ramp reaches zero load. The rise in load during the recovery hold, ΔF, is the difference of the 15-point running median of the load between 2 s before the final movement and 60 s after the start of the hold. Its uncertainty $u = \sqrt{\pi/15}\, s_F$ is that of the difference of two such medians under an independent-sample approximation, with s_F the standard deviation of the load about its running median in the last ten minutes of the hold, and it quantifies short-term load-channel noise. The deflection δ_2 is the crosshead position at which the 3-point running median of the load first falls to 1 N on the final movement. In test 1, where the load is smallest, the 5-point median and 1.5 N are used.

S7.3 Rig stiffness

The loading and unloading ramps of the eleven tests resolve the elastic stiffness of the bar in the rig. The stiffness was taken as the slope of load against crosshead position between 10 and 60 % of F_{app} on loading and between 90 and 10 % of $F_{8\mathrm{h}}$ on unloading, which gives 22 values. A joint fit of their logarithms to a beam of span L with shear compliance (shear correction factor 5/6, Poisson's ratio 0.33, $E = 65.2$ GPa) in series with a constant machine compliance C_m gives $L = (141.8 \pm 1.7)$ mm and $C_m = (1.06 \pm 0.61) \times 10^{-4}$ mm/N, with an rms residual of 7.4 % in the logarithm of stiffness. The uncertainties are the standard deviations over 2000 bootstrap resamples

of the tests. The stiffness windows of 5 to 30 % with 90 to 50 %, and of 30 to 60 % with 50 to 10 %, give $L = (142.5 \pm 3.3)$ mm and (141.8 ± 2.8) mm with rms residuals of 21 and 17 % in the logarithm of stiffness. The fitted span exceeds the nominal span of 140 mm by (1.8 ± 1.7) mm, so the drawn value is not excluded, and the fitted value is used in every calculation below. The machine compliance is 0.6, 2.9 and 10.9 % of the total compliance of the 3, 5 and 8 mm bars. Without it, fits of the span alone give 141.9, 143.4 and 147.4 mm for the three thicknesses.

A second feature of the rig matters more. The linear part of each loading ramp, extrapolated to zero load, meets the displacement axis between −0.09 and 0.70 mm. The toe, taken from a straight line through the ramp between 20 and 60 % of F_{app}, is largest for two of the 3 mm bars (0.70 and 0.42 mm). Seating of this kind, if it continues during the hold, lowers the load at a fixed crosshead position and appears as an apparent relaxation. Section S11.3 examines its signature in the residuals.

S7.4 Repeatability

In the uniaxial series the four specimens that overlap during the first 1.93 hours of the plotted holds span a band of width 0.0057, 0.0097 and 0.0049 % in strain at 137.5, 150 and 162.5 MPa, averaged over the first 1.3 hours. At 1.3 hours the width is 10 to 17 % of the inelastic strain.

Tests 2 and 5 were repeated. In test 2 the second run reached 5.26 mm against 5.47 mm at nearly the same peak load and relaxed by 36.51 % against 41.27 %. In test 5 it reached the same deflection at 545.9 N against 512.9 N and relaxed by 29.86 % against 22.73 %. The differences of 4.8 and 7.1 percentage points set the scale of the variability between repeated tests.

S7.5 Springback and load recovery of the bending tests

Supplementary Table S21: Springback and load recovery of the eleven bending tests, as defined in Section 2.5, with $k_0 = F_{\mathrm{app}}/\delta_0$.

test	h (mm)	instantaneous springback (%)	final protocol springback (%)	deflection recovery (%)	load recovery (%)
1	3	58.1	61.3	7.6	11.5
2	3	61.7	70.9	23.9	8.5
3	3	52.4	58.9	13.6	11.9
4	5	70.5	76.1	18.8	5.4
5	5	65.7	71.6	17.2	7.3
6	5	70.2	77.1	23.0	7.6
7	5	67.5	74.6	21.7	6.8
8	5	62.4	70.1	20.5	7.6
9	8	77.5	83.2	25.2	5.2
10	8	73.8	80.0	23.5	4.7
11	8	63.3	69.7	17.3	6.7

S7.6 Bending records used in the calculations

The present calculations follow the recorded bending histories, with a loading speed of about 0.0667 mm/s. The recovered load of the earlier study (Yang, 2017) denotes the final reaction, whereas ΔF here is the rise from a specified baseline.

S8 Comparison with the dislocation-density model and thermodynamic basis

S8.1 Comparison with the dislocation-density model

The earlier study describes the same alloy and tests with a single inelastic strain rate, a normalised mobile dislocation density that carries the back stress, a normalised immobile density, a precipitate radius and two hardening variables, in equations (5.22)–(5.29) with 19 fitted constants (Yang, 2017). Those equations are implemented here with the printed constants, in the units that reproduce the published creep and recovery curves of that study,

and run without refitting on the records of Section 2.2. The last five equations are driven by the creep rate and do not enter the first three, so creep, recovery and back stress depend on eight of the 19 constants.

On the 204 strain residuals of the uniaxial identification of Section 4.2 the dislocation-density model gives an objective of 147 against 1.95 for the present law, an rms error of 0.012 against 0.0014 %, and on the stress record at fixed strain an rms error of 3.33 against 4.17 MPa, Fig. S11. It reaches the measured recovered strain after eight hours, 0.038 against 0.035 % for the raw record at 162.5 MPa, but by the wrong path. Its reverse flow is the hyperbolic sine of the back stress, and that back stress saturates during the hold at the level that arrests the forward creep, so after unloading the recovery starts at 1.5×10^{-7} per second and reaches 0.003 % in the first four minutes where the record reaches 0.018. At fixed strain the same saturation carries the recovered stress above the measured eight-hour reaction to 19.3 MPa at eight hours and 22.3 MPa at fifty hours. Its recovered strain changes little with hold time, and that comparison returns in Sections 7.1 and 9.1.

The two models share a stress-driven hyperbolic-sine response and an internal opposing stress, and differ in what carries the back stress and how it decays. In the dislocation-density model the back stress is a power of a saturating dislocation density, and its decay is the reverse creep itself. Here σ_b is the stiffness H times the recoverable strain, its decay is the return of that strain at a rate set by the same stiffness, and the permanent branch uses elapsed time in place of an explicit ageing state. The present law is a separately identified macroscopic benchmark of the strain response.

The threshold law of Yang (2026) places the elastic spring in series with two parallel rails. The flow rail has a time-evolving threshold, while the back-stress rail has a spring with dynamic recovery and a static-recovery dashpot. With the threshold and dynamic recovery removed and the static-recovery time taken to infinity, the rails reduce to the back-stress element of Fig. 4, with H as the hardening modulus. The present law keeps the autonomous ageing of the threshold law as the time-hardening factor on the permanent branch. The two laws read the fixed-strain record differently. The threshold law takes the eight-hour reaction as the back stress at the end of the hold, whereas in the present law that reaction is a stage of a continuing recovery, and the back stress at unloading follows from the zero-stress record through H.

For the present isothermal assessment, the internal strains start from zero before loading, and the coefficients remain fixed at 174 °C. The zero initial strains define the reference state for the calculation and do not imply a dislocation-free specimen.

S8.2 Thermodynamic basis

The law has the structure of a generalised standard material (Halphen and Nguyen, 1975; Germain et al., 1983). With the elastic strain $\varepsilon - \varepsilon_b - \varepsilon_v$, the Helmholtz free energy per unit volume is

$$\psi = \tfrac{1}{2} E\,(\varepsilon - \varepsilon_b - \varepsilon_v)^2 + \tfrac{1}{2} H\,\varepsilon_b^2, \tag{S9}$$

so that $\sigma = \partial\psi/\partial\varepsilon$ returns Eq. (1) and the thermodynamic forces conjugate to the two inelastic strains are

$$X_b = -\frac{\partial\psi}{\partial\varepsilon_b} = \sigma - \sigma_b, \qquad X_v = -\frac{\partial\psi}{\partial\varepsilon_v} = \sigma. \tag{S10}$$

The back stress is the force $H\varepsilon_b$ stored in the spring, and the force that drives the back-stress dashpot is the applied stress less that stored force. All rate coefficients and moduli are positive. The isothermal Clausius–Duhem inequality requires $\mathcal{D} = \sigma\dot{\varepsilon} - \dot{\psi} = X_b\dot{\varepsilon}_b + X_v\dot{\varepsilon}_v \geq 0$.

Both flow rules follow from one dual dissipation potential,

$$\begin{aligned}\Omega^*(X_b, X_v, t) = {} & \frac{A_b}{B_b}\big[\cosh(B_b X_b) - 1\big] \\ & + \frac{A_v}{B_v}\big[\cosh(B_v X_v) - 1\big]\,(1 + t/\tau_v)^{-p},\end{aligned} \tag{S11}$$

through $\dot{\varepsilon}_b = \partial\Omega^*/\partial X_b$ and $\dot{\varepsilon}_v = \partial\Omega^*/\partial X_v$, which return Eqs. (2) and (3). At every instant the potential is convex in the forces, non-negative, and zero at zero force. The dissipation is therefore non-negative branch by branch,

$$\mathcal{D} = A_b\,X_b \sinh(B_b X_b) + A_v\,X_v \sinh(B_v X_v)\,(1 + t/\tau_v)^{-p} \geq 0. \tag{S12}$$

The time-hardening factor scales the permanent-flow potential by a positive function of time, so convexity and the sign of $\mathcal{D}$ do not depend on it. Equation (S12) holds for either sign of X_b. The back-stress dashpot dissipates

while it flows backwards as it does while it flows forwards, and the second law places no obstacle in front of recovery at zero stress. The energy $\frac{1}{2}H\varepsilon_b^2$ stored in the spring is dissipated in the dashpot as the recoverable strain returns.

A threshold on the reverse flow is admissible too. The potential

$$\begin{aligned}\Omega_Y^* = \frac{A_b}{B_b}\Big[\cosh(B_b\langle|X_b| - \Delta\sigma_Y\rangle) - 1\Big] \\ + \frac{A_v}{B_v}\big[\cosh(B_vX_v) - 1\big]\,(1 + t/\tau_v)^{-p},\end{aligned} \tag{S13}$$

with $\langle\cdot\rangle$ the Macaulay bracket and $\Delta\sigma_Y$ a threshold that may grow with ageing time, is convex, vanishes on the dead band $|X_b| \le \Delta\sigma_Y$ and gives $\dot\varepsilon_b = A_b\,\mathrm{sgn}(X_b)\sinh(B_b\langle|X_b| - \Delta\sigma_Y\rangle)$ with $X_b\dot\varepsilon_b \ge 0$. Thermodynamics admits the gated law and the ungated law alike and does not choose between them. The choice rests on the reverse drive at zero stress, which is $-\sigma_b$, and on whether its magnitude lies inside the dead band. A threshold blocks recovery only if the reverse drive remains within that dead band. Section 5 tests this condition by re-identifying the law at different fixed thresholds.

The back stress here differs in its specified role from the kinematic variable of the Armstrong–Frederick and Chaboche models (Armstrong and Frederick, 1966; Chaboche, 1993, 2008). There it translates an elastic domain of finite extent, so that reverse flow starts only when the drive leaves the domain, and it evolves by its own hardening, dynamic recovery and static recovery terms. Here σ_b is the stiffness H times the recoverable strain, there is no domain to leave, and the decay of σ_b is the return of that strain. Precedents for flow without a dead band are the unified viscoplastic models that have no yield surface (Hart, 1976; Bodner and Partom, 1975), in which inelastic flow is not switched off below a stress threshold.

S9 Analytical solutions

S9.1 Constants of recovery at zero stress and in the bent bar

Supplementary Table S22: Closed-form constants of the recovery at zero stress for the 8 hour holds, from the CART-only parameters. $s_0 = B_b\sigma_b^0$, t^* is the onset time of the logarithmic stage of Eq. (8) and t_{90} is the time at which 90 % of the recoverable strain has returned. The last three columns give t_{90} for the CART-only identification (none added) and for the two joint identifications of Table 3, with the SRBT tests added to the identification listed.

					t_{90} (h), SRBT added		
σ (MPa)	σ_b^0 (MPa)	σ_b^0/σ	s_0	t^* (s)	none	3, 6, 10	4, 8, 9
137.5	121.8	0.886	7.20	51	10.2	5.4	4.5
150	134.3	0.895	7.94	24	9.3	5.0	4.1
162.5	146.8	0.903	8.68	12	8.6	4.6	3.8

The straight line ends when s approaches unity. Between 10 s and 3×10^4 s the exact solution at 162.5 MPa falls by 0.031 %, an average of 0.0038 % per unit $\ln t$ that lies below the asymptotic slope because the curve bends away from its asymptote towards the end of the window. The record underlying Fig. 3a falls by 0.031 %, which is 0.0039 % per unit, over the same eight logarithmic units. At zero stress 90 % of the recoverable strain has returned after 8.6–10.2 h and 99 % after 1.3 days. The time scale follows $1/A_b$. The joint identifications of Section 7 raise A_b by factors of 1.9 and 2.2, which shortens the time for 90 % of the recoverable strain to return at 162.5 MPa to 4.6 and 3.8 h, while the slope $1/(B_bH)$ changes by 4 and 2 %. The time scale is thus known to a factor of about two and the slope to a few per cent.

In the bent bar each fibre obeys Eq. (2) with a stress set by the compatibility of the section, Section 6.1. During the recovery stage of tests 4, 8 and 11, with the bar held at the deflection at which the model's load reaches zero (Section 6.3), the section solver gives for the outer fibre at midspan a stiffness K_d of 0.97, 1.00 and 0.98 times $E + H$, evaluated as the change in drive over the change in recoverable strain between the start and the end of the stage. The outer-fibre comparisons approximate the homogeneous fixed-strain limit over the checked interval, and Eq. (5) with $K_d = E + H$ follows the magnitude of their drive to within 0.5, 1.1 and 0.8 MPa as

it falls from 87, 167 and 174 MPa at the start of the stage, on the conditioned path, to between 17 and 18 MPa. Section equilibrium, rig compliance and contact govern the complete bending response, so neither homogeneous limiting time is a universal structural recovery time.

S10 Comparison with viscoelastic and threshold models

S10.1 Logarithmic recovery and loss of recovered stress

A logarithmic tendency does not rule out a linear spectrum (Mainardi and Spada, 2012). A positive retardation density per unit $\log \tau$ proportional to $\exp(-a/\tau)$, for example, gives a recovery after a hold of duration T proportional to

$$R(t) = \log(1 + t/a) - \log\{1 + t/(a + T)\}, \tag{S14}$$

which is logarithmic for $a \ll t \ll T$. Nor is the eventual loss of a recovered stress peculiar to a spectrum. Integrated through the CABT history, the complete sinh law reaches a maximum of 20.0 MPa after 29.6 h and then declines as the permanent flow continues under the recovered stress. The calculation checks the law at a duration beyond the tests, and the analytical rest value of 20.7 MPa holds only with the permanent strain frozen.

S11 Beam analysis and apparatus checks

S11.1 Peak loads and recovery loads

The predicted peak loads differ from the measured ones by −11.3 to +22.0 %, −7.0 to +9.4 % over the 5 and 8 mm bars, with a mean absolute error of 6.6 %, which is the error of the ramp-based rig model together with the inelastic flow during the ramp. The conditioned final recovery loads for tests 7, 8 and 11 are 73, 78 and 191 N against 64, 80 and 182 N from the smoothed records at the common endpoint, and the same calculations driven by the unmodified crosshead end at 55, 21 and 63 N. The complete measured and calculated histories are shown in Fig. S7.

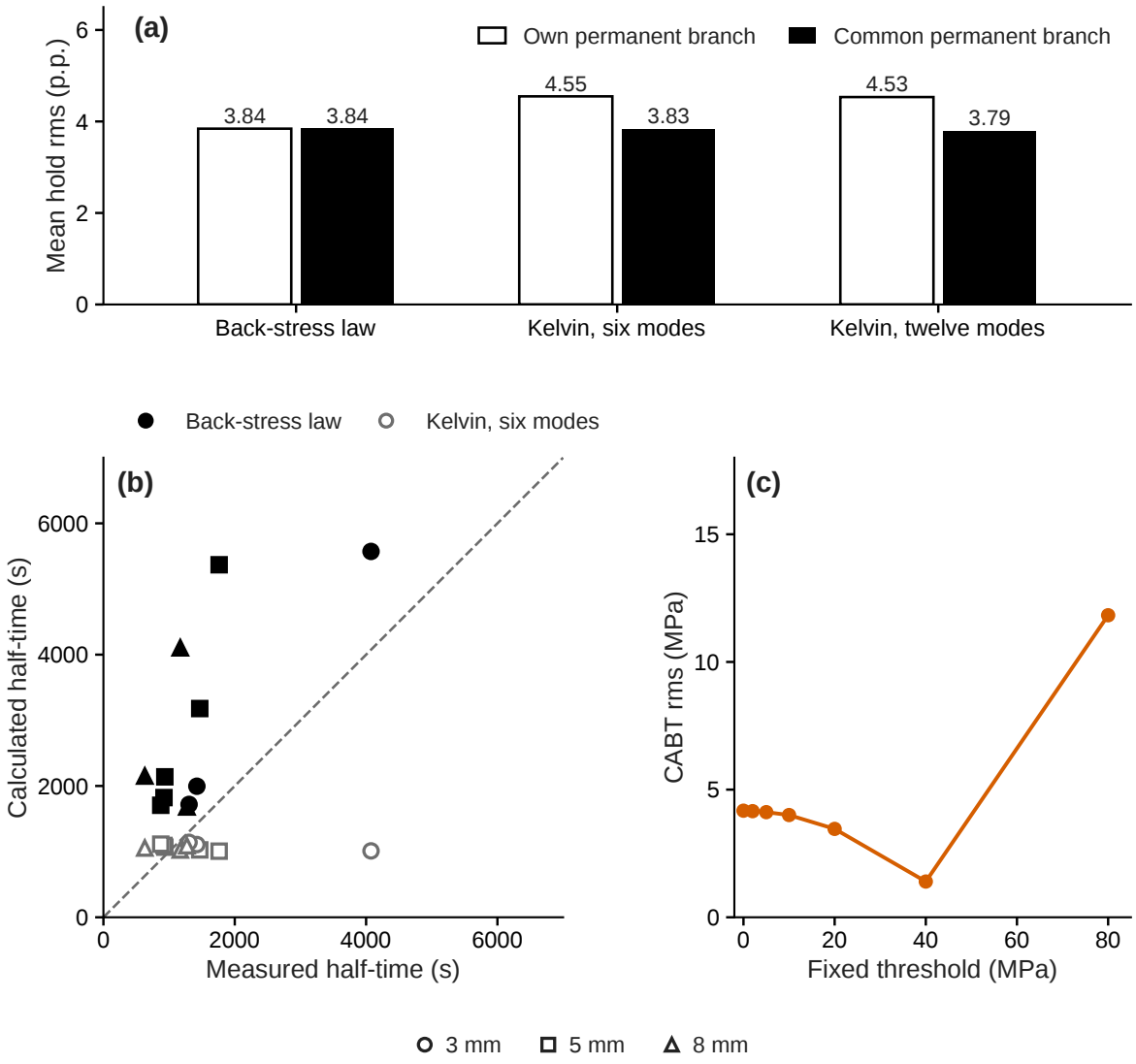
S11.2 Through-thickness fields during the hold

The calculated fields describe stress redistribution within test 8 during the hold (Fig. S16). Inelastic flow during the loading ramp already changes the elastic stress profile. At its end the outermost quadrature fibre carries 379 MPa near the surface. Within the first hour the outer fibres relax to 225 MPa while the load falls to 73 % of its initial value, and at eight hours the surface stress stands at 183 MPa, 48 % of its initial value, against 60 % for the load and 76 % for the fibre at mid-depth. The load is the moment of the fibre stresses, so its relaxation ratio is a weighted mean of theirs. The surface relaxes further than the load and the interior less, and once the inelastic strain has concentrated at the surface no single ratio converts the recorded load into a surface stress. The permanent strain at the surface reaches 0.62 % at eight hours, six times the inelastic strain of the identification set, while the recoverable strain stays between 0.052 and 0.060 %, close to its saturation value σ/H, because the back stress follows the fibre stress through the hold. The law has no threshold, so every fibre flows and the inelastic strain falls smoothly to zero at the neutral axis. There is no elastic core.

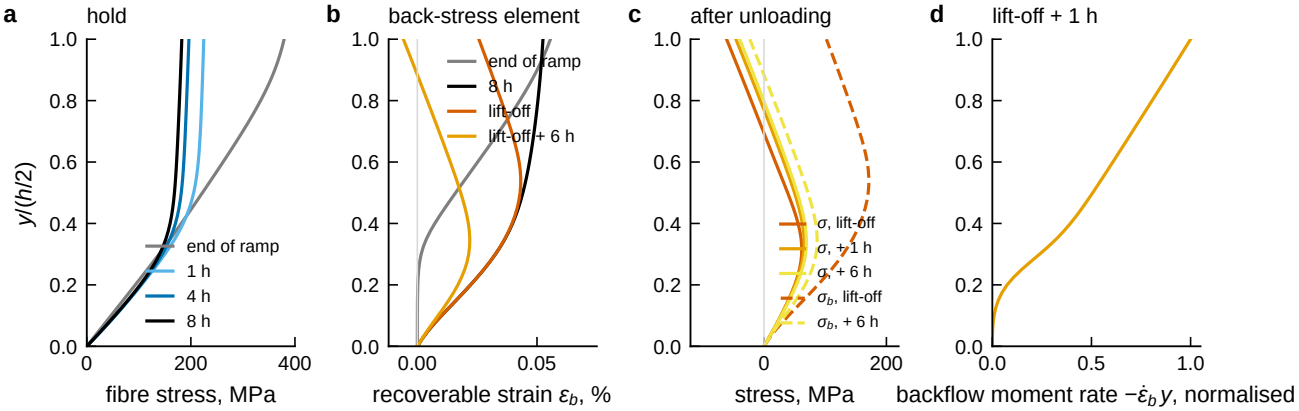
S11.3 Displacement offsets at small deflection

A displacement taken up by supports or contact changes the bar deflection at fixed crosshead. In the linear section model a shift u_s changes the load by u_s/C, where $C = L^3/(48EI) + L/(4\kappa Gbh) + C_m$. Using the nominal secant stiffness $k_0 = F_{\mathrm{app}}/\delta_0$ gives the approximate diagnostic scale $100u_s/\delta_0$ in percentage points of relaxation. The measured crosshead does not separate support motion from specimen deformation.

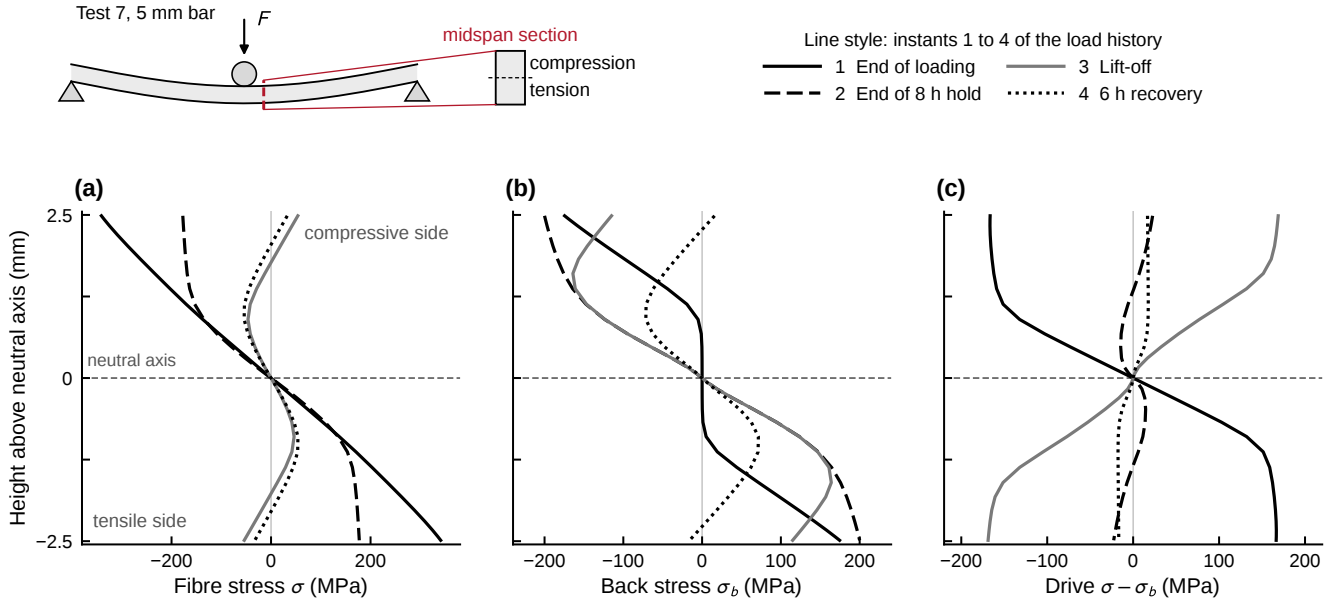
Figure S8b compares the excess relaxation over the model with the excess permanent crosshead deflection, $100\Delta\delta_2/\delta_0$, for the eight 5 and 8 mm bars, with $r = 0.84$ and a slope of 0.81. Both axes contain the prediction of the same law and share the geometry and displacement inputs, so the correlation is consistent with a displacement offset of the kind the ramp toes show without being an independent measure of it. The subtraction illustrated in Fig. S8a is the corresponding model-dependent decomposition. Separating apparatus motion from constitutive error needs a direct measurement of the bar deflection and of the support motion.



Supplementary Figure S15: Comparison of the recoverable laws, showing (a) mean hold errors, (b) calculated versus measured half-times and (c) CABT errors at fixed symmetric thresholds. The hold-error bars distinguish independently fitted and common permanent branches. Half-times use the original fits and the dashed line denotes equality. Every threshold fit uses CART data alone.



Supplementary Figure S16: Through-thickness fields of the section model at the station nearest midspan, test 8 (5 mm, 442 MPa), from the CART-only identification. (a) Fibre stress during the hold. (b) Recoverable strain ε_b through the hold, at lift-off and six hours later. (c) Residual stress σ and back stress σ_b after unloading. (d) Contribution of each fibre to the rate of recovery of the load, $-\dot{\varepsilon}_b\, y$, one hour after lift-off.



Supplementary Figure S17: Through-thickness profiles at the midspan section of test 7, above and below the neutral axis, at the instants of Fig. 7. (a) Fibre stress, (b) back stress and (c) drive $\sigma - \sigma_b$. Line style distinguishes the instants, and the sketch locates the section.

S12 Fitting with bending tests included

Two joint identifications add bending tests 3, 6 and 10 (one bar of each thickness) or tests 4, 8 and 9 (5, 5 and 8 mm) to the three CART histories, and the second and third rows of Table 3 give their results. The bending residuals use thirty times per hold and per recovery interval, with one percentage point of normalised load weighted as 0.001 % strain. The fits drive the bar with the recorded crosshead throughout, including the unloading, rather than with the event-conditioned path of Section 6.3, so they measure the compromise needed to fit the recorded responses under that input. The remaining bending histories and the CABT were withheld, and the shorter CART tests remain partially dependent through their contribution to the pooled hold bands.

In both joint fits the back-stress stiffness and stress sensitivity move much less than the prefactor. B_b changes by −1 and −2 % and H by −3 and +0.4 % between the CART-only and the two joint identifications, so the slope $1/(B_b H)$ of the logarithmic stage changes by +4 and +2 %, while A_b rises by factors of 1.9 and 2.2 and shortens the recovery time scale by the same factors (Section 4.3). The stress sensitivity of the permanent flow falls by 10–14 %, from $B_v = 0.0288$ to 0.0260 and 0.0249 MPa^{-1}, and the exponent p halves while the prefactor A_v falls by a factor of 1.8 to 2.7. Those last two parameters move along the correlated direction noted in Section 4.2, and Fig. S8d shows that the rate function they define is unchanged inside the stress window of the uniaxial tests. At 150 MPa and one hour the three identifications give permanent-flow rates of 2.1×10^{-8}, 1.9×10^{-8} and 2.0×10^{-8} s^{-1}. They diverge above about 200 MPa, by a factor of two at 300 MPa and three at 442 MPa, where the joint identifications, which see the surface fibres of the high-load bars, flow more slowly. The price is paid in the uniaxial hold-outs. The CABT error rises from 4.17 MPa to 6.91 and 6.95 MPa in the two joint identifications (Table S18), and the CART hold-out error in creep strain rises from 0.0019 to 0.0028 %, while the remaining bending tests improve by one to three percentage points in eight-hour relaxation.

A fixed-B_v profile gives a further view of the extrapolation. Fixing B_v at 0.020 or 0.012 MPa^{-1} and re-identifying the remaining CART parameters raises the CART objective from 1.95 to 7.4 or 29 and reduces the excess high-load bending relaxation. One sinh permanent branch with a single stress sensitivity therefore does not cover 137.5–442 MPa.

Set against the ranges of Table 5, the joint identifications move B_b and H by at most 1.1 local scales of the CART curves (Section S3), A_b by 4.3 and 5.5, B_v by 6.2 and 8.6 and p by −17 and −14. B_v falls to 0.0260 and 0.0249 MPa^{-1}, below both the profile range and the LOSO range, which gives the slower permanent flow above 200 MPa. τ_0 falls to 5.3 and 4.4 h, below the LOSO range and, in the second fit, below the profile range, a factor of about two from the CART-only value. B_b and H stay inside their profile ranges. p falls below its profile range in both fits and A_v in the first, while both stay inside the LOSO range, along the correlated direction whose rate function is unchanged inside the uniaxial window. The bending records therefore add the stress sensitivity of the permanent flow at high stress and shorten the recovery time scale.

S13 Numerical details

The controlled CART identifications use exact constant-stress solutions, with 204 strain residuals scaled by 10^4. The sinh law has six free parameters and fixes $\tau_v = 10$ s. Refitting the other six parameters with τ_v fixed at 1, 100 and 1000 s changes the objective by −0.3, +2.3 and +12.7 %. Bounds are $A_b \in [10^{-14}, 10^{-3}]$ and $A_v \in [10^{-16}, 10^{-3}]$ s^{-1}, $B_b \in [0.005, 1]$ and $B_v \in [0.001, 0.5]$ MPa^{-1}, $H \in [1, 10^4]$ GPa and $p \in [0, 3]$. The Kelvin spectra retain nonnegative amplitudes and use the same permanent-branch exponent and stress-sensitivity bounds. Eight sinh starting points and fifteen Kelvin starting pairs converge to their respective reported objectives. Fixed-threshold profiles re-identify all six parameters with four starts per threshold. In the isolated-branch comparison of Table 4 the Kelvin amplitudes with a fixed permanent branch are a nonnegative linear least-squares problem solved once, and the sinh branch with a fixed permanent branch is refitted in A_b, B_b and H from six starts. The restricted spectra of Section 5 use the same variable-projection fit with retardation times of 1 to 10^4 s and 0.1 to 10^4 s. Independent Radau integration agrees with the constant-stress solutions to better than 10^{-12} strain for the tested cases. The ageing-stiffness variant of Section 9.1 has no closed form and is fitted with Radau integration of every residual from three starting values of q, which converge to the same minimum.

Bending uses six Gauss stations along the half-span and eight through the positive half-thickness, with symmetric compressive fibres. LSODA integrates the rate equations at relative tolerance 10^{-7} and absolute strain tolerance 2×10^{-13}. Unloading endpoint corrections are solved by a bracketed scalar root with reintegration of each trial ramp. Comparisons with 10×12 and 16×20 Gauss grids on tests 1, 3, 4, 8 and 11 change sinh

recovered loads by less than 0.03 %. A frictionless-roller finite-rotation sensitivity uses the integrated relation between curvature and tangent angle while retaining the same constitutive and shear laws. Run on the three 3 mm bars and on test 8, it changes the peak loads by less than 0.8 %, the hold errors by at most 0.25 percentage points and the recovered loads by less than 0.1 % relative to the small-rotation calculation. The unloading shift is converged until the signed reaction at the ramp endpoint is zero to better than 0.0001 N.

Every bending result of Section 6, Table S1, Table 4 and the recovery comparisons comes from one evaluation, in which the peak and end-of-hold loads are taken at the stage instants and the unloading shift u_s is solved by a bracketed root with reintegration of the ramp, as in Section 6.3.

One-at-a-time apparatus checks with the CART-only constants vary the effective span from 140.1 to 143.5 mm and the machine compliance from 0.45 to 1.67×10^{-4} mm/N, which are the one-standard-deviation limits of the ramp fits of Section 2.4. Among tests 4, 8 and 11 the predicted six-hour rise changes by up to 6.4 % and the predicted peak load by up to 5.4 % of the prediction at the reported apparatus, both for test 11 at the lower compliance limit. The largest peak error of any of these scenarios is 6.8 % of the measured peak, for test 4 with a span of 143.5 mm, and it includes the peak error of that test at the reported apparatus (Table S10). The ranges of Section 6.3 and Fig. 6 repeat these checks for all eleven tests with the same constants, spans of 140 and 146 mm about the fitted 141.8 mm and the same compliance limits, in an independent implementation of the section model in the dimensionless variables $\sigma/162.5\,\mathrm{MPa}$ and t/τ_0, integrated by LSODA at relative tolerance 10^{-9}, which reproduces the reported evaluation of all eleven tests to 1.4×10^{-6} relative. The unloading secant compliances of the individual records span 0.85 to 8.6×10^{-4} mm/N, far wider than the ramp fit, and at the upper end the six-hour ratio of test 9 falls to 0.45 (Table S8). Moving the stage instants themselves by one second and re-conditioning the model lets it lift off before the recorded stop and takes the six-hour ratio of test 9 to 0.24. That case measures the sensitivity to the event on which the model is conditioned and is kept outside the ranges as a conditioning choice. Profiles of the CART objective refit the remaining parameters at each grid point from the global minimum and from the neighbouring point, four starts each, and leave-one-stress-out refits use eight starts. Pure-bending projections use 32 Gauss fibres over the positive half-thickness, checked against 16 and 64 fibres. Compensation is solved directly for retained curvature, with a maximum target residual below 3×10^{-12} mm^{-1}.

The joint identifications use the recorded crosshead and their own residual weighting and parameter bounds, including an admissible negative lower bound for p. Their fitted p values are positive.

S14 Half-times on other time windows

The main text compares recovery rates on a common window, from 60 s to six hours after unloading. Two other conventions appear in the records and in earlier analyses, and both are given here.

Counted to the end of each record, the half-time is the first time after unloading at which the normalised recovery R reaches 0.5, with R equal to 1 at the end of the record, taken for SRBT as the median of its last 200 samples. R is zero at the unloading load minimum for CABT, at the first resolved point for CART and at the start of the recovery hold for SRBT. The CABT endpoint is fixed at eight hours. The half-times are 195 s for CART and 676 s for CABT. For the eight 5 and 8 mm SRBT records, half-times are evaluated on the 15-point running median of the load. Seven give 360–758 s, while test 4 gives 848 s. That record re-crosses the half level until 3180 s, and tests 5 to 8 show shorter periods of re-crossing. These values depend on the starting point and the endpoint of each record and do not rank the constraints.

Normalising the two uniaxial records at 162.5 MPa to run from zero at 300 s to one at eight hours, the first half crossings occur 2169 s after unloading for strain and 4276 s for stress, a ratio of 1.97, where the law gives 2904 and 2780 s, a ratio of 0.96. The law gives the same ratio on the common window, and the measured ratio is 2.5 there.

S15 Recovery rates under different constraints

For homogeneous recovery at zero applied stress, linearisation of Eq. (2) about zero recoverable strain gives

$$\dot{\varepsilon_b} \simeq -A_b B_b H \varepsilon_b, \qquad \tau_0 = (A_b B_b H)^{-1}. \tag{S15}$$

For homogeneous fixed-strain recovery, the stress instead satisfies

$$\dot{\sigma} = -E(\dot{\varepsilon}_b + \dot{\varepsilon}_v). \tag{S16}$$

If permanent flow is suppressed for this local comparison, perturbations about equilibrium decay according to

$$\delta\dot{\varepsilon}_b = -A_b B_b (E + H)\delta\varepsilon_b, \qquad \tau_\varepsilon = [A_b B_b (E + H)]^{-1}. \tag{S17}$$

With the CART-only constants and $E = 65.2\,\mathrm{GPa}$, these limiting times are approximately 9.56 h and 8.21 h, respectively. The fixed-strain estimate applies near equilibrium with permanent flow suppressed. The complete CABT law includes permanent flow and must be integrated as a coupled system. For the beam, equilibrium and compatibility couple the fibre states through Eq. (11), so neither scalar time is a universal structural recovery time.

References

P. J. Armstrong and C. O. Frederick. A mathematical representation of the multiaxial Bauschinger effect. Technical Report RD/B/N731, Central Electricity Generating Board, 1966. Reprinted in Materials at High Temperatures 24 (2007) 1–26.

S. R. Bodner and Y. Partom. Constitutive equations for elastic-viscoplastic strain-hardening materials. *Journal of Applied Mechanics*, 42(2):385–389, 1975. doi: 10.1115/1.3423586.

J.-L. Chaboche. Cyclic viscoplastic constitutive equations, part I: a thermodynamically consistent formulation. *Journal of Applied Mechanics*, 60(4):813–821, 1993. doi: 10.1115/1.2900988.

J. L. Chaboche. A review of some plasticity and viscoplasticity constitutive theories. *International Journal of Plasticity*, 24:1642–1693, 2008. doi: 10.1016/j.ijplas.2008.03.009.

P. Germain, Q. S. Nguyen, and P. Suquet. Continuum thermodynamics. *Journal of Applied Mechanics*, 50(4b): 1010–1020, 1983. doi: 10.1115/1.3167184.

B. Halphen and Q. S. Nguyen. Sur les matériaux standard généralisés. *Journal de Mécanique*, 14:39–63, 1975.

E. W. Hart. Constitutive relations for the nonelastic deformation of metals. *Journal of Engineering Materials and Technology*, 98:193–202, 1976. doi: 10.1115/1.3443368.

Francesco Mainardi and Giorgio Spada. On the viscoelastic characterization of the jeffreys–lomnitz law of creep. *Rheologica Acta*, 51:783–791, 2012. doi: 10.1007/s00397-012-0634-x.

Yo-Lun Yang. *A study of inelastic/anelastic behaviour and springback of AA7050 alloy in creep age forming*. PhD thesis, Imperial College London, 2017.

Yo-Lun Yang. Competitive hardening dynamics in viscoplastic materials with evolving threshold stress. SSRN preprint, 2026.